UNR/CSDE1 drives a post-transcriptional program to promote melanoma invasion and metastasis

Laurence Wurth[1,2], Panagiotis Papasaikas[1,2], David Olmeda[3], Nadine Bley[4], Guadalupe T. Calvo[3], Santiago Guerrero[1,2], Daniela Cerezo-Wallis[3], Javier Martinez-Useros[5], María García-Fernández[3], Stefan Hüttelmaier[4], Maria S. Soengas[3] and Fátima Gebauer[1,2*]

(1) Gene Regulation, Stem Cells and Cancer Programme, Centre for Genomic Regulation (CRG), The Barcelona Institute of Science and Technology, 08003-Barcelona, Spain

(2) Universitat Pompeu Fabra (UPF), 08003-Barcelona, Spain

(3) Molecular Oncology Programme, Spanish National Cancer Research Centre (CNIO), 28029-Madrid, Spain

(4) Sect. Molecular Cell Biology, Institute of Molecular Medicine (IMM), Martin-Luther-University (MLU), 06120-Halle, Germany

(5) Translational Oncology Division, Oncohealth Institute - Health Research Institute - University Hospital "Fundacion Jimenez Diaz", 28040-Madrid, Spain

(*) Corresponding author:

Tel: +34-93 3160120

Fax: +34-93 3969983

E-mail: fatima.gebauer@crg.eu

Summary

RNA binding proteins (RBPs) modulate cancer progression through poorly understood mechanisms. Here we show that the RBP UNR/CSDE1 is over-expressed in melanoma tumors and promotes invasion and metastasis. iCLIP-Seq, RNA-Seq and ribosome profiling combined with in silico studies unveiled sets of pro-metastatic factors coordinately regulated by UNR as part of RNA regulons. In addition to RNA steady state levels, UNR was found to control many of its targets at the level of translation elongation/ termination. Key pro-oncogenic targets of UNR included *VIM* and *RAC1*, as validated by loss and gain of function studies. Our results identify UNR as an oncogenic modulator of melanoma progression, unravel the underlying molecular mechanisms, and identify potential targets for this therapeutically challenging malignancy.

Significance

RNA binding proteins (RBPs) are gaining great attention in cancer research for their potential to regulate essentially every hallmark of tumor development. Yet, the molecular mechanisms that underlie these capacities are unclear, particularly in aggressive cancers such as melanoma, where RBPs remain largely uncharacterized. Our work establishes that the RBP UNR/CSDE1 is a critical modulator of melanoma metastasis, and reveals a network of UNR targets including both well-known cancer drivers as well as genes not previously linked to the disease. Our data broaden the functions of UNR, unveiling a role in translation elongation/ termination, and highlight the physiological relevance of RBP-mediated control of oncogenic networks in cancer.

Introduction

Melanoma is an increasingly prevalent cancer that remains a paradigm of genetically and histopathologically heterogeneous diseases (Shadendorf et al., 2015). Both benign and malignant lesions can share dysplastic features that greatly complicate diagnosis. Despite great progress in dermoscopic techniques, staging is still largely defined on the basis of the thickness of the primary melanocytic lesion, although this criterium is long-known to be subject to error (Thompson et al., 2004). Activating alterations in key signaling cascades (e.g. driven by BRAF or MEK) have resulted in the development of molecularly guided therapies, but response rates are frequently transient (Flaherty et al., 2012). Inhibitors of checkpoint blockers such as CTLA-4, PD1 or PDL1 are providing unprecedented durable responses, although only to a fraction of metastatic melanoma patients (Bathia and Thompson, 2016). Thus, the melanoma field is in need of diagnostic and prognostic biomarkers, as well as of new targets for drug development.

High-throughput sequencing efforts have revealed massive heterogeneity of the melanoma transcriptome (Dutton-Regester and Hayward, 2012). Despite this defining property, RNA-related mechanisms remain surprisingly understudied. A comprehensive analysis of RNA binding proteins (RBPs) and their targets in the context of melanoma initiation and progression seems lacking. RBPs are particularly relevant because they can modulate every post-transcriptional step of gene expression, from splicing in the nucleus to mRNA export, localization, translation or decay in the cytoplasm. Each single RBP can bind to hundreds of mRNAs, forming extensive networks in which functionally related genes may be co-regulated, representing

"RNA regulons" (Morris et al., 2010). As a result, RBP malfunction may have dramatic consequences for cell physiology. Indeed, RBPs are emerging as critical modulators of cancerous traits, yet little is known about the underlying mechanisms and key downstream targets (Wurth and Gebauer, 2015).

Upstream-of-N-Ras (UNR), known as CSDE1 in mammals, is a conserved RBP containing five cold-shock domains (CSDs) that bind single stranded RNA (Goroncy et al., 2010; Triqueneaux et al., 1999). UNR locates primarily in the cytoplasm, where it regulates mRNA translation and stability (reviewed in Mihailovich et al., 2010). In *Drosophila*, UNR inhibits cap-dependent translation of *msl-2* mRNA and modifies the structure of *roX2* long non-coding RNA, both events contributing to the regulation of X-chromosome dosage compensation (Abaza et al., 2006; Duncan et al., 2006; Militti et al., 2014). In the case of *msl-2*, UNR binds to the 3' UTR together with the RBP SXL, establishing extensive intertwined interactions that explain cooperative RNA recognition (Hennig et al., 2014). In the case of *roX2*, UNR can bind on its own. Thus, UNR binding requirements and regulatory mechanisms may vary depending on the target transcript. The versatile binding of UNR to RNA likely underlies the diverse biological roles of this protein. In mammals, UNR may either promote or inhibit apoptosis and differentiation depending on cell type (Dormoy-Raclet et al., 2007; Elatmani et al., 2011; Horos et al., 2012).

RNA immunoprecipitation (RIP) analysis revealed that *Drosophila* UNR binds to hundreds of transcripts (Mihailovic et al., 2012). Among these, mRNAs encoding conserved regulators related to human cancer progression were identified (e.g. *TGFB1*, *ABL1* or *CTNNB1*). The targets of mammalian UNR have not been described

at genome-wide level. However, the small list of known targets suggests a potential role of UNR in proliferation and cancer progression. For example, UNR participates in the destabilization of *FOS* mRNA by binding to its coding sequence (CDS) (Chang et al., 2004). In addition, UNR regulates internal ribosome entry site (IRES)-dependent translation of the transcripts encoding the oncogene MYC, the cell cycle kinase PITSLRE and the apoptosis regulator APAF-1 (Evans et al., 2003; Mitchell et al., 2003; Tinton et al., 2005). Furthermore, UNR represses the translation from its own IRES, providing a negative feedback loop to temper the levels of UNR along the cell cycle (Schepens et al., 2007).

Here, we have evaluated the potential role of UNR in cancer progression using melanoma as a model system.

Results

UNR promotes melanoma cell invasion and metastasis

To obtain insights into a potential role of UNR in cancer progression, we first interrogated the TCGA database for alterations of *CSDE1/UNR* expression in a variety of human cancer samples. *CSDE1* mRNA is upregulated in a high percentage of tumors, especially in skin and ovary cancers (Figure S1). We therefore focused on melanoma as a prototypic skin cancer. Because UNR negatively regulates its own translation (Schepens et al., 2007), RNA levels may not correlate with protein amounts. Hence, we monitored the levels of UNR protein in melanoma cell lines and tissue specimens. We found that UNR was over-expressed in a variety of melanoma cell lines compared to normal melanocytes. Importantly, we also observed high

expression of UNR in primary and metastatic lesions from melanoma patients compared to benign nevi (Figure 1A-B).

An inducible shRNA system was then used to conditionally deplete UNR from a representative melanoma cell line (SK-Mel-103) characterized by its aggressive and metastatic properties (Figure 2A, left panel). A cumulative growth assay, which monitors proliferation in a confluence-independent manner, showed no differences between control and UNR-depleted cells (Figure 2A, middle panel). However, a reduction in cell number was observed when cells reached confluency (Figure 2A, right panel, and S2A). Furthermore, while control cells were able to grow as spheres, UNR-depleted cells remained tightly attached to the surface (2A, right insets). These results suggest that UNR influences proliferation under stress conditions such as crowding. UNR depletion reduced the clonogenic capacity of melanoma cells and their ability to grow in soft agar (Figure 2B-C), results that were recapitulated in different melanoma cell lines characterized by prototypical genetic mutations (Figure S2B). Unless otherwise indicated, we henceforth used SK-Mel-103 cells. Restoring the expression of UNR in depleted cells using a cDNA resistant to shRNA inhibition rescued colony formation in soft agar, indicating that impaired colony formation upon UNR depletion is unlikely to result from off-target effects of the shRNA (Figures 2C and S2C). In addition, enforced expression of UNR in cancerous cells increased colony formation, suggesting that the dosage of UNR is important for colony growth (Figure S2C, right panel). These results suggest that UNR promotes anchorage-independent growth. This was further confirmed by growing cells in suspension. Contrary to control cells, UNR-depleted cells were unable to grow detached from the surface and underwent cell death as measured by caspase 3/7 cleavage activity (Figures 2D and S2D-E), suggesting that UNR promotes resistance to anoikis.

Additionally, UNR depletion resulted in decreased migration of cells within collagen (Figure 2E).

Anchorage-independent growth, migration and resistance to anoikis are frequently associated with invasive and metastatic capacities of tumor cells. To evaluate these properties more directly, we cultured melanoma spheroids in matrigel and measured their invasion index. UNR-depleted cells formed significantly smaller spheroids with dramatically reduced invasion index (Figures 2F and S2F). To investigate how general these effects were, we depleted UNR in a number of melanoma cell lines and cells from other tumor origins (breast and ovarian cancer), carrying either wild-type or mutated *BRAF*, a gene frequently mutated in melanoma. In all cases, depletion of UNR favoured anoikis and reduced the invasive capacities of cells (Figure S2H). Conversely, over-expression of UNR augmented these traits (Figure S2H). These results indicate that UNR promotes tumorigenesis in vitro.

Next, we validated the pro-tumorigenic functions of UNR in vivo, using xenograft models in mice. To this end, UNR-depleted SK-Mel-103 melanoma cells were implanted subcutaneously in immunodeficient mice. As shown in Figure 2G, UNR-depleted cells resulted in smaller tumors compared to control cells. To assess for UNR-roles in surrogate models of metastasis, control and UNR-depleted cells were labeled with luciferase to monitor tumor growth and dissemination upon tail-vein injection. The results showed a striking reduction of the metastatic capacity of UNR-depleted cells to the lung, a frequent site for melanoma metastasis in mice (Figure 2H). For a more direct assessment of metastatic potential, mice were injected subcutaneously, and lymph nodes proximal and distal to the site of injection were monitored for the presence of tumor cells. Depletion of UNR from highly metastatic

SK-Mel-103 cells indeed eliminated lymph node metastasis (Figure 2I). Conversely, overexpression of UNR in otherwise non-metastatic UACC-257 cells promoted migration and invasion in vitro, as well as lymph node metastasis formation in vivo (Figures 2I and S2G). Taken together, the data indicate that UNR is required to sustain the invasive and metastatic capacity of melanoma cells.

Identification of UNR targets by iCLIP-Seq

To unravel the mechanisms by which UNR promotes invasion and metastasis, we intersected three types of high-throughput analysis: i) iCLIP-seq to identify direct RNA targets of UNR, ii) RNA-Seq and iii) ribosome profiling to determine at which level UNR regulates the expression of its targets (Figure 3A).

To perform iCLIP-Seq (Konig et al., 2011), an anti-UNR antibody was generated that immunoprecipitates endogenous UNR efficiently and with high specificity (Figure 3B, left panel, and Figure S3A). After UV-crosslink of melanoma cells and partial RNA digestion, UNR-RNA complexes were immunoprecipitated and appeared as a smear over the UNR band in a protein gel (Figure 3B, right panel, red square). No complex was present in control lanes lacking UV-crosslinking or immunoprecipitated with rabbit IgG, indicating specificity (lanes 1,2). In addition, upon extensive digestion with RNase, the signal of the complex was reduced to a sharp band close to the molecular weight of UNR (lane 4) that was barely detectable in UNR-depleted cells (lanes 5-6). We performed two independent iCLIP experiments which showed a high correlation (Figure S3B; see Table S1 for iCLIP statistics), revealing a set of 1532 common targets (Figure 3C and Table S2). Most of these targets are protein-coding RNAs, while only few long-non-coding RNAs were identified. Strikingly, 18.5% of the common targets overlap with *Drosophila* UNR targets previously

identified by RIP-Seq (Mihailovic et al., 2012), which is considerable given the strong divergence between the two species (Table S2), suggesting conserved functions for UNR. The vast majority of the remaining targets have not been previously described in the literature. Of the known targets of mammalian UNR, only *PABPC1* and *CSDE1* mRNAs were retrieved in our system. Binding of UNR to its own mRNA occurred preferentially at the 5' UTR, consistent with the proposed role of UNR regulating translation from its own IRES (Schepens et al., 2007) (Figure 3D). However, unlike previous reports, binding to *PABPC1* mRNA was detected preferentially at the 3' UTR (Figure 3D), suggesting potential additional regulatory mechanisms of this transcript (Patel et al., 2005). Identified UNR targets included a significant fraction of ribosomal protein and histone mRNAs, among others (Table S2). Gene Ontology (GO) analysis showed enrichment for endoplasmic reticulum-associated translation, extracellular components, exosome, cell junctions, focal adhesions or melanosome, which fit well with functions of UNR in invasion and metastasis (Figure S3C and Table S3). Interestingly, of the 1532 UNR targets, 396 were found linked to cancer development (Table S2). Validation of a subset of these targets by independent RNA-IP experiments showed an 89% validation rate (Figure S3D). Thus, a high proportion (26%) of UNR targets encode cancer-related factors previously unknown to be regulated by this RBP.

UNR binding properties

iCLIP enrichment of UNR targets showed a general correlation with RNA abundance, suggesting relaxed sequence binding requirements for this protein (Figure 3E). Binding is nevertheless specific, as many highly abundant transcripts were not bound by UNR. DREME analysis identified a consensus binding motif similar to that

described by in vitro SELEX experiments (Triqueneaux et al., 1999) (Figure 3F). UNR binds mature mRNA, preferentially in the CDS and the 3' UTR and to a lesser extent in the 5' UTR, suggesting functions for UNR in addition to its described roles as an IRES trans-acting factor (ITAF) (Figure 3G). Overall, the binding motif is centered around the UNR iCLIP peaks; however, when different regions of the mRNA are considered separately, a strong tendency for the motif to be located in the center of the iCLIP tags is detected for CDS peaks but not for 5' or 3' UTR peaks, suggesting different binding modes of UNR to these regions (Figure S3E). RNA structural analysis using experimental PARS (Parallel Analysis of RNA Structure) data shows a drop in the PARS score at UNR peaks, indicating that UNR binds single stranded RNA (Figure S3F) (Wan et al., 2014). In addition, UNR targets show significantly decreased PARS scores compared to all transcripts, indicating a preference of UNR for unstructured mRNAs (Figure 3H). Metagene analysis of the position of UNR binding along the mRNA shows preference of binding downstream of the start and/or stop codons, as well as at the stop codon (Figure 3I). This binding profile is specific for UNR, as we did not observe it for other RBPs such as HuR or TDP43 (Figure S3G).

UNR regulates the levels of transcripts encoding oncogenes and tumor suppressors

Binding by an RBP does not necessarily imply regulation of the bound target at the tested condition. To identify iCLIP targets regulated by UNR, we first undertook RNA-Seq analysis of cells where UNR had been depleted for 5 days compared to shControl pairs. To obtain complete information about coding and non-coding RNAs, we performed RNA-Seq on both poly(A)-RNA and total RNA after ribozero

treatment, each in duplicate. The duplicates showed high correlation (Figure S4A, see also Table S1 for statistics). Because UNR binds mostly mature mRNAs, we focused our analysis on poly(A) RNA-Seq. For histone mRNAs, which lack poly(A) tails, we used total RNA-Seq.

Evaluation of iCLIP enrichment and RNA abundance changes showed a poor correlation, indicating that only a reduced number of binding targets were regulated by UNR at the steady state level (Figure 4A). A total of 715 genes showed altered RNA levels, 93 of which were direct UNR targets (Figure 4B). Comparatively more mRNAs were downregulated upon UNR depletion, suggesting prevalent roles of UNR as an activator of mRNA accumulation (Figure 4B). Gene ontology analysis of regulated iCLIP targets (other than histones and ribosomal protein mRNAs) showed over-representation of cell adhesion and extracellular matrix components (Figure 4C and Table S4). We selected iCLIP targets encoding factors involved in these functions for validation and observed consistent downregulation of tumor-promoting factors upon UNR depletion, while tumor-suppressing factors were upregulated (Figure 4D). A transcript downregulated by UNR encodes the tumor suppressor PTEN, a gene whose expression is frequently reduced in melanoma. We find upregulation of PTEN both at the mRNA and protein levels upon UNR depletion (Figure 4D and S4B).

Finally, we tested whether the regulation of mRNA levels by UNR was associated with a specific binding pattern of UNR along the transcript. Interestingly, a meta-analysis indicated strong positioning of UNR at the stop codon of regulated transcripts (Figure 4E). mRNAs upregulated upon UNR depletion (i.e. downregulated by UNR) showed additional binding of UNR at the start codon.

In summary, UNR regulates the steady state levels of mRNAs coding for tumor promoting and suppressing factors in a manner that correlates with its oncogenic properties.

UNR regulates critical melanoma genes at the translation level

Given that UNR binds to a subset of melanoma transcripts, we expected this protein to be an mRNA-specific regulator. To rule out indirect effects on global translation, we analyzed de novo protein synthesis by ^{35}S-metabolic labeling as well as polysome profiling of shUNR versus shControl cells. We did not detect significant differences in global translation by any of these assays (Figure S5A).

To identify genes regulated by UNR at the translation level, we performed ribosome profiling (RP), a technology that provides quantitative and positional information of ribosomes along transcripts at codon resolution (Ingolia et al., 2009). Three independent RP experiments were performed on shUNR and shControl cells after 5-day induction of the shRNA. These experiments showed a good correlation (Figure S5B). Metagene analysis indicated that reads mapped primarily at the CDS, ending abruptly at the stop codon and extending to some degree into the 5' UTR, typical of RP. In addition, single nucleotide resolution analysis revealed the triplet (codon) pace of the ribosome, attesting to the quality of our data (Figure S5C). Our coverage was nevertheless limited, as low abundant genes could not be quantified with statistical significance (see Table S1). For example, beta-catenin (*CTNNB1*) mRNA appears as "not translationally regulated" by our statistical analysis. However, western blot analysis showed that the levels of CTNNB1 decrease upon UNR depletion even in the presence of proteasome inhibitors, suggesting that UNR promotes *CTNNB1* translation (Figure S5D, left panel).

The details of our RP analysis are described in Extended Experimental Procedures (see also Figure S5E). Briefly, we performed three types of analyses: i) we considered all transcripts and normalized the number of ribosome protected fragments (RPFs) with their RNA levels (translational efficiency or "TE" group); ii) we excluded transcripts changing at the steady-state level and quantified normalized RPFs ("RPF" group); iii) we analyzed the distribution of ribosomes along the mRNA, even for transcripts that did not change at the TE or RPF levels ("Distribution" group). Altogether, the analysis revealed 451 genes regulated at the translation level, of which 127 are UNR iCLIP targets (Figure 5A and Tables S5-S6). Gene Ontology analysis of UNR targets (excluding histone and ribosomal protein mRNAs) showed enrichment in categories related to extracellular matrix among others (Figure 5B and Table S5).

A summary of all changes observed upon UNR depletion is shown in Figure 5C. In this graph, mRNA abundance change is plotted against changes in the number of RPFs. Quadrants a and c are the most populated, and show genes for which there is a positive correlation between mRNA abundance and translation, while almost no changes are detected in the anti-correlation quadrants d and b. These results nicely illustrate that our ribosome profiling data reproduce events observed at the RNA-Seq level. However, most UNR direct targets (orange crosses) fall outside these quadrants and are present in the green, pink and white areas. The green regions represent genes that change at the mRNA steady state level without significant differences in RPF reads. Transcripts in these regions show differences in amount that are not reflected at the level of ribosome association and, therefore, these transcripts are translationally compensated. A significant proportion of UNR targets fall in these areas, most of which correspond to histone mRNAs.

The pink areas show genes that do not change at the mRNA level but at the RPF level. We anticipate that these genes are regulated at the level of translation initiation, which results in changes in the number of ribosomes associated to the mRNA. As UNR has been shown to regulate translation initiation, we expected most of the UNR iCLIP targets in these areas. Surprisingly, however, this is not the case. As shown in Figure 5C, multiple genes do not change neither at the mRNA nor RPF levels (middle white square). Interestingly, these genes display changes in the relative distribution of ribosomes along the CDS (black dots). Most of these transcripts are direct UNR targets (orange crosses). Altogether, of the 127 direct UNR targets regulated at the translation level, 20 (16%) show changes only in RPF levels while 60 (47 %) display changes only in ribosome distribution (Table S5). Changes in ribosome distribution without accompanying changes in RPF levels likely reflect regulation at the translation elongation or termination steps. Thus, these results suggest that, unexpected from previous literature, UNR regulates translation of its melanoma targets mainly at the level of elongation or termination. Consistently, in addition to sub-polysomal fractions, UNR was found associated to early translating ribosomes in sucrose gradients (Figure S5F).

Similar to transcripts regulated at the steady state level (Figure 4), examination of the UNR binding profile in transcripts showing differential ribosome distribution revealed a stronger positioning around the start and/or stop codons (Figure 5D). In addition, transcripts downregulated by UNR at the RPF level showed a shift of UNR binding towards the 5' UTR.

To validate our RP analysis we first selected *TRIO*, a gene encoding a Rho Guanine nucleotide Exchange factor (GEF) involved in uveal melanoma (Vaqué et al., 2013). *TRIO* is a direct UNR target that shows reduced RPF levels upon UNR depletion

without accompanying changes at the RNA level, suggesting decreased translation initiation (Table S5). Indeed, Western blot analysis confirmed downregulation of TRIO protein in UNR-depleted cells (Figure S5G). We further focused on two genes that are highly altered in malignant melanoma, *VIM* (Vimentin) and *RAC1* (Ras-related C3 botulinum toxin substrate 1). VIM is a component of intermediate filaments that furnishes cells with resilience to changes in shape and is a marker of ephitelial-to-mesenchymal transition (EMT), while RAC1 is a GTPase belonging to the Ras superfamily with pleiotropic effects. Both proteins are important for invasion and metastasis (Bid et al., 2013; Satelli and Li, 2011). *VIM* and *RAC1* are regulated at the level of ribosome distribution, with no changes in RNA amounts or crude RPFs (Table S5). Analysis of RP data indicated a re-distribution of ribosomes towards the 5' end in UNR-depleted cells for both transcripts, suggesting that they are translationally stimulated by UNR at the level of elongation (Figure 5E). Indeed, Western blot analyses revealed a strong downregulation of these proteins in UNR-depleted cells (Figure 5E). Downregulation of VIM and RAC1 in the absence of UNR persisted in the presence of proteasome inhibitors, indicating a role for UNR in synthesis and not stability of these proteins (Figure S5D, middle and right panels). To confirm regulation after translation initiation, we performed ribosome run-off assays using metabolic labeling. Newly synthesized VIM was monitored for 10 min after inhibition of translation initiation with Harringtonine. In these conditions, synthesis of VIM was strongly downregulated in UNR-depleted cells, while synthesis of Tubulin and Vinculin was marginally affected (Figure 5F). In order to investigate the mechanism further, we performed reporter assays. Our iCLIP data indicate that UNR binds primarily to the 3' UTR of *VIM* mRNA (Figure 5G). Transfection assays with

mRNA reporters containing or lacking *VIM* 3' UTR confirmed that UNR upregulates *VIM* at the level of translation by binding to the 3' UTR (Figure 5G).

In conclusion, ribosome profiling provides a list of cancer relevant genes regulated by UNR at the level of translation, including critical melanoma genes. In addition, the data identify a role of UNR in translation elongation/ termination.

Regulation of *VIM* and *RAC1* mRNA translation by UNR promotes cancerous traits

To identify candidate downstream effectors of UNR in melanoma progression, we performed network analyses. We retrieved melanoma-relevant genes from the MelGene (Athanasiadis et al., 2014), Cosmic Cancer Gene Census (Futreal et al., 2004) and KEGG CANCER (Kanehisa and Goto, 2000; Kanehisa et al., 2014) databases, in addition to individual publications (see Supplemental data for a complete list of references) and constructed a curated list of 74 "melanoma genes". These genes are highly mutated in melanoma and/or reported to control tumorigenic features of melanoma cells (Table S7). This list was intersected with UNR regulated iCLIP targets to build a network with interaction data from Pathway Commons (Cerami et al., 2011) using the Cytoscape 3.1.1 platform (Shannon et al., 2003). The interactions include physical interactions (including co-occurrence in a complex), co-regulation and molecular modification.

Strikingly, 66% of the melanoma genes are connected directly or indirectly with UNR targets (Figure 6A). Among these targets we find 15 genes that are also "melanoma genes" (*VIM, RAC1, PTEN, B2M, CCL2, CTTN, CXCL8, CYR61, FN1, MAPRE1, MIF, SDC4, TNC, TRIO* and *YBX1*). Thus, 15 out of 45 UNR targets in the network have a direct implication in melanoma. Other targets are involved in cancer

progression but currently unknown to play a role in melanoma (*HNRNPA2B1*, *IER3*, *GNAI2*, *HMGA1*, *YWHAQ*, *YWHAE*, *ADAM12*, *EIF4A2*, *PABPC1*, *EIF4G2*) while the remaining targets have not been previously related to cancer progression. These results highlight the potential of UNR to influence multiple aspects of melanoma biology, as well as the potential of the network to uncover activities involved in melanoma progression. Among the targets, we find coherent sets of activities influencing melanoma cell survival, invasion and metastasis (Figure 6A, blue and red boxes), identifying post-transcriptional regulons coordinated by UNR in melanoma development (see Discussion).

In order to assess the relevance of selected UNR targets in melanoma progression, we first checked whether their levels changed according to their expected regulation by UNR in the same set of cells previously scored for anoikis resistance and invasion. We found that UNR depletion reduced the levels of VIM and RAC1 in most cells, while it increased the levels of PTEN (Figure 6B). Conversely, mild over-expression of UNR increased VIM and decreased PTEN levels, while the effect on RAC1 was more variable (Figure 6B). Taken together, these results indicate that the levels of VIM, RAC1 and PTEN are consistently regulated by UNR across a panel of cell lines. To assess whether translational regulation by UNR was relevant for melanoma progression, we tested whether over-expression of the translational targets *VIM* and *RAC1* could overcome the defects in anchorage independent growth resulting from UNR depletion. As control we selected *LOXL2*, a gene involved in cancer cell invasion and also regulated by UNR (Figure 4D), but not present in the network (Figure 6A). As expected, depletion of UNR dramatically reduced the number and size of colonies that grow in soft agar (e.g. Figure 7A). While LOXL2 over-expression did not show a significant effect (Figure 7A), VIM and RAC1 over-

expression fully restored colony growth and number (Figure 7B). These results indicate that regulation of *VIM* and *RAC1* mRNA translation by UNR contributes to melanoma traits. Furthermore, the results validate the potential of the network to uncover activities involved in melanoma progression.

Discussion

RBPs are fundamental players in RNA metabolism, but their contributions to disease are only starting to be recognized (Castello et al., 2013; Darnell, 2010; Wurth and Gebauer, 2015). Here we show that the RBP UNR plays key roles in melanoma progression, identify relevant mRNA targets and investigate the underlying mechanisms.

Perhaps the most unanticipated role of UNR found in this study is primarily related to melanoma invasion and metastasis, as shown in xenograft models in mice. Consistent with these results, our data indicate that UNR promotes anoikis resistance, migration and invasion in cultured melanoma cells. Most strikingly, over-expression of UNR alone converted a non-metastatic melanoma cell into a metastatic one. In agreement with this, genome-wide and functional analyses revealed that UNR regulates a series of targets with GO terms enriched in extracellular matrix and cell adhesion components. Binding of UNR to its targets follows a particular pattern, with strong UNR positioning closely downstream of the Start and/or Stop codons. This binding pattern prevails even after removing abundant classes of transcripts that are bound by UNR, such as ribosomal protein or histone mRNAs. Although the significance of this positioning is currently unclear, it seems specific for UNR, because other well-known post-transcriptional regulators (HuR and TDP43) do not show the same binding

pattern. Interestingly, binding of UNR shifts precisely to the Start and/or the Stop codons in regulated transcripts, suggesting that regulation by UNR is associated to recognition of these defining landmarks of the CDS.

A group of targets regulated by UNR en mass at the mRNA and translation levels encode histones. While histone mRNAs are downregulated upon UNR depletion, this is compensated for by an increase in their translational efficiency. Compensatory mechanisms seem to be commonplace when UNR perturbations are introduced in the cell, warning for careful validation of endogenous protein levels when either mRNA amounts or translational efficiencies are considered in isolation. In addition, most transcripts showing changes are not direct UNR targets, indicating considerable secondary effects.

Our unbiased analysis revealed targets regulated by UNR at the level of translation initiation, consistent with the location of bulk UNR in non-polysomal fractions. A selective group of those shows preferential UNR binding at the 5' UTR. Given the reported role of UNR as an ITAF (Evans et al., 2003; Mitchell et al., 2003; Schepens et al., 2007; Tinton et al., 2005), these transcripts may represent targets containing undefined IRESs which may impact on melanoma progression. Nevertheless, the largest group of translationally regulated transcripts seems to be controlled after the initiation step. The accumulation of ribosomes at the 5' of the CDS of many of these targets in the absence of UNR, and the fact that UNR associates with the first few polysomal fractions in sucrose gradients, suggest a role of UNR in early elongation.

Although most reports on translational regulation have focused on initiation (reviewed in Sonenberg and Hinnebusch, 2009), regulation of translation elongation is emerging as a mechanism important in situations of proteotoxic stress or heat shock (Liu et al., 2013; Shalgi et al., 2013). Few RBPs with roles in translation elongation

have been reported. These include FMRP, hnRNP E1 and the PUF-AGO complex, all of which inhibit elongation by various mechanisms (Darnell et al., 2011; Friend et al., 2012; Hussey et al., 2011). For example, hnRNP E1 and the PUF-AGO complex bind to the 3' UTR of target transcripts and interfere with the elongation factor eEF1A1 to prevent its release from the ribosome or block its GTPase activity, respectively. The hnRNPE1 mechanism is especially relevant for breast cancer progression, as TGF-beta promoted phosphorylation of hnRNP E1 results in translation de-repression and contributes to EMT (Hussey et al., 2011). Remarkably, our results show that UNR activates -rather than represses- elongation, at least of *VIM* and *RAC1* mRNAs. Stimulation of translational elongation of these transcripts by UNR contributes to the malignant properties of melanoma cells. The precise molecular mechanism by which UNR promotes elongation, and how UNR activity is regulated during melanoma development are important questions for future research.

A network analysis was performed to reveal UNR regulated targets directly involved in melanoma progression. The results uncovered 15 UNR targets that have previously been implicated in melanoma progression. Among these we find important downstream effectors of driver oncogenes that contribute to melanoma cell survival, invasion and metastasis. For instance, the c-Jun proto-oncogene is a transcription factor hyper-activated in malignant melanoma (reviewed in (Kappelmann et al., 2014). Two of the most relevant downstream effectors of c-Jun are the tumor suppressor PTEN and the inflammatory factor CCL2 (c-Jun downregulates *PTEN* and upregulates *CCL2* to promote cell survival and metastasis (Hettinger et al., 2007; Qian et al., 2011; Wolter et al., 2008). UNR does not target c-Jun directly, but downregulates *PTEN* and upregulates *CCL2* mRNAs, providing a post-transcriptional

mimic of the transcriptional c-Jun effect. These transcripts constitute an RNA regulon coordinated by UNR.

Another RNA regulon is composed of the transcripts encoding *SDC4*, *RAC1*, *TRIO*, *TNC*, *FN1*, *CTTN* and *VIM* . SDC4 is a transmembrane receptor that connects the extracellular matrix with intracellular signaling pathways (Elfenbein and Simons, 2013). SDC4, as well as the guanine exchange factor TRIO, activate the small GTPase RAC1, which relays signals to the cytoskeleton to modulate adhesion and migration. Indeed, the activation of these factors has been linked to metastatic melanoma (Feng et al., 2014; Krauthammer et al., 2012; Ridgway et al., 2010). TNC and FN1 are proteins of the extracellular matrix that also interact with SDC4 to modulate cell adhesion. TNC over-expression has been related with melanoma invasion and metastasis, while FN1 upregulation suppresses motility of melanoma cell lines (Novak et al., 2015; Shao et al., 2015). CTTN binds actin and is required for the formation of invadopodia in invasive tumoral cells (Ayala et al., 2008) whereas, as mentioned above, VIM is a component of intermediate filaments that preserves the mechanical integrity of cells during invasion (Satelli and Li, 2011). All of these factors are coordinately regulated by UNR in a direction consistent with invasion and metastasis: UNR promotes the translation of *RAC1*, *TRIO* and *VIM* mRNAs and upregulates *SDC4*, *TNC* and *CTTN* transcript levels, while it represses the translation of the *FN1* message. These results reveal RNA regulons coordinated by UNR to modulate invasion and metastasis.

In addition to melanoma genes regulated by UNR, the network shows extensive connections of UNR targets with a large proportion of melanoma genes not directly regulated by UNR. Some of these targets are involved in progression of other tumor types while others have not been shown to contribute to cancer. For instance,

ADAM12 is a metalloprotease involved in restructuring cell-cell and cell-matrix interactions that is upregulated by UNR, but whose function in melanoma has not been addressed. It will be interesting to test the contribution of ADAM12 to the acquisition of melanoma cancerous traits.

In summary, our data identify an oncogenic function for UNR, uncover UNR targets and mechanisms of regulation, and provide a resource of potential melanoma biomarkers and therapeutic targets.

Experimental Procedures

Normal and malignant melanocytic cells, molecular and cell biology techniques, list of oligonucleotides, high-throughput methods and detailed computational analysis are described in Extended Experimental Procedures. All sequencing was performed on Illumina HiSeq2000 (single read, 50nts) at either the EMBL or the CRG Genomics Core facilities.

Ethics Approvals

All experimental animal procedures were approved by the Institutional Ethics Committees (CEEA) of the PRBB, the CNIO and the Instituto de Salud Carlos III, and met the guidelines of Catalonian (Catalan law 5/1995 and Decrees 214/97, 32/2007) and European (EU directives 86/609 and 2001–486) regulations, as well as the Standards for Use of Laboratory Animals A5388-01 (NIH).

Human tumor biopsies were obtained from the i+12 Biobank (RD09/0076/00118) of the Hospital 12 de Octubre and the Spanish Hospital Biobank Network, under ethical protocols approved by their Clinical Investigation Ethical Committees. Procedures

with human melanocytes were approved by the Ethical Committees of the CNIO and the Hospital 12 de Octubre. All human samples were obtained after informed consent form the patient.

RNA-Seq

Gene expression differences between shUNR and shControl cells were measured using poly(A)+ RNA sequencing, except for histones, for which we used ribozero-treated total RNA sequencing. Libraries were sequenced, mapped to the hg19 human genome using Tophat2 and analyzed for differential gene expression using Cuffdiff2 (Trapnell et al. 2013). The p value threshold for differential gene expression calling was set to 0.005.

iCLIP-Seq

iCLIP was performed as described (König et al 2010). Libraries were sequenced, mapped using Bowtie2 (Langmead et al. 2012) and corrected for amplification bias. Peaks were called using HOMER (http://homer.salk.edu/homer/) and motif analysis was performed using DREME (Bailey et al. 2011).

Ribosome profiling

Ribosome profiling was performed according to (Ingolia et al 2012). Details on Ribosome profiling data analysis including pre-processing mapping and centering, differential crude RPF, translational efficiency and ribosome distribution calculations can be found in Extended Experimental Procedures.

Accession Numbers

The ArrayExpress accession numbers for the RNAseq, iCLIP and ribosome profiling experiments are E-MTAB-3805, E-MTAB-3818 and E-MTAB-3815, respectively.

Author Contributions

F.G. conceived the project. Experimental data were contributed as follows: D.O., G.T.C, D.C-W., J.M-U., M.G-F., Figures 1, 2H-I; S.G., Figures 5G, 6A, S1; N.B., Figures 2D-F, S2D-H and 6B; L.W. performed all other experimental work and P.P. provided bioinformatical analysis of all high-throughput data. S.H., M.S.S. and F.G. supervised the project. L.W., P.P. and F.G. wrote the manuscript. All other authors edited the manuscript.

Acknowledgements

We thank Laura Battle and Olga Coll for technical assistance with xenograft experiments, José Luis Rodríguez-Peralto and Pablo Ortiz-Romero (Anatomical Pathology and Dermatology Services as the Hospital 12 de Octubre) for tissue procurement, and Corine Bertolotto for Mel-ST cells. We thank the CRG and EMBL Genomics Facilities for high-throughput sequencing, and the CRG Protein Service for recombinant UNR expression. We are grateful to Anne Willis for the human UNR cDNA, to Jernej Ule and Elías Bechara for advice on iCLIP, and to Nick Ingolia, Sebastian Leidel and Danny Nedialkova for advice on ribosome profiling. We thank Juan Valcárcel, Johan Tisserand and Jesús García-Foncillas for useful discussions and comments on the manuscript. L.W. was supported by the Fonds National de la Recherche, Luxembourg, and cofounded by the Marie Curie Actions of the European Commission (FP7-COFUND) (Project Code 1072489). M. G-F was supported by a Juan de la Cierva fellowship from the Spanish Ministry of Economy and Competitiveness (MINECO).

This work was supported by MINECO and the European Regional Development Fund (ERDF) under grant BFU2012-37135 to F.G., and Consolider CSD2009-00080 and TV'13-20131430 (Marató de TV3) grants to F.G. and M.S.S. We acknowledge support of the Spanish Ministry of Economy and Competitiveness, 'Centro de Excelencia Severo Ochoa 2013-2017', SEV-2012-0208 (to CRG) and SEV-2011-0191 (to CNIO).

Authors declare no conflicts of interest.

References

Abaza, I., Coll, O., Patalano, S., and Gebauer, F. (2006). Drosophila UNR is required for translational repression of male-specific lethal 2 mRNA during regulation of X-chromosome dosage compensation. Genes Dev *20*, 380-389.

Athanasiadis, E.I., Antonopoulou, K., Chatzinasiou, F., Lill, C.M., Bourdakou, M.M., Sakellariou, A., Kypreou, K., Stefanaki, I., Evangelou, E., Ioannidis, J.P., *et al.* (2014). A Web-based database of genetic association studies in cutaneous melanoma enhanced with network-driven data exploration tools. Database (Oxford) *2014*.

Ayala, I., Baldassarre, M., Giacchetti, G., Caldieri, G., Tete, S., Luini, A., and Buccione, R. (2008). Multiple regulatory inputs converge on cortactin to control invadopodia biogenesis and extracellular matrix degradation. J Cell Sci *121*, 369-378.

Bathia, S., and Thompson, J.A. (2016). PD-1 Blockade in Melanoma: A Promising Start, but a Long Way to Go. JAMA *315*, 1573-1575.

Bid, H.K., Roberts, R.D., Manchanda, P.K., and Houghton, P.J. (2013). RAC1: an emerging therapeutic option for targeting cancer angiogenesis and metastasis. Mol Cancer Ther *12*, 1925-1934.

Castello, A., Fischer, B., Hentze, M.W., and Preiss, T. (2013). RNA-binding proteins in Mendelian disease. Trends Genet *29*, 318-327.

Cerami, E.G., Gross, B.E., Demir, E., Rodchenkov, I., Babur, O., Anwar, N., Schultz, N., Bader, G.D., and Sander, C. (2011). Pathway Commons, a web resource for biological pathway data. Nucleic Acids Res *39*, D685-690.

Chang, T.C., Yamashita, A., Chen, C.Y., Yamashita, Y., Zhu, W., Durdan, S., Kahvejian, A., Sonenberg, N., and Shyu, A.B. (2004). UNR, a new partner of poly(A)-binding protein, plays a key role in translationally coupled mRNA turnover mediated by the c-fos major coding-region determinant. Genes Dev *18*, 2010-2023.

Darnell, J.C., Van Driesche, S.J., Zhang, C., Hung, K.Y., Mele, A., Fraser, C.E., Stone, E.F., Chen, C., Fak, J.J., Chi, S.W., *et al.* (2011). FMRP stalls ribosomal translocation on mRNAs linked to synaptic function and autism. Cell *146*, 247-261.

Darnell, R.B. (2010). RNA regulation in neurologic disease and cancer. Cancer Res Treat *42*, 125-129.

Dormoy-Raclet, V., Markovits, J., Malato, Y., Huet, S., Lagarde, P., Montaudon, D., Jacquemin-Sablon, A., and Jacquemin-Sablon, H. (2007). Unr, a cytoplasmic RNA-binding protein with cold-shock domains, is involved in control of apoptosis in ES and HuH7 cells. Oncogene *26*, 2595-2605.

Duncan, K., Grskovic, M., Strein, C., Beckmann, K., Niggeweg, R., Abaza, I., Gebauer, F., Wilm, M., and Hentze, M.W. (2006). Sex-lethal imparts a sex-specific function to UNR by recruiting it to the msl-2 mRNA 3' UTR: translational repression for dosage compensation. Genes Dev *20*, 368-379.

Dutton-Regester, K., and Hayward, N.K. (2012). Reviewing the somatic genetics of melanoma: from current to future analytical approaches. Pigment Cell Melanoma Res *25*, 144-154.

Elatmani, H., Dormoy-Raclet, V., Dubus, P., Dautry, F., Chazaud, C., and Jacquemin-Sablon, H. (2011). The RNA-binding protein Unr prevents mouse embryonic stem cells differentiation toward the primitive endoderm lineage. Stem Cells *29*, 1504-1516.

Elfenbein, A., and Simons, M. (2013). Syndecan-4 signaling at a glance. J Cell Sci *126*, 3799-3804.

Evans, J.R., Mitchell, S.A., Spriggs, K.A., Ostrowski, J., Bomsztyk, K., Ostarek, D., and Willis, A.E. (2003). Members of the poly (rC) binding protein family stimulate

the activity of the c-myc internal ribosome entry segment in vitro and in vivo. Oncogene *22*, 8012-8020.

Feng, X., Degese, M.S., Iglesias-Bartolome, R., Vaque, J.P., Molinolo, A.A., Rodrigues, M., Zaidi, M.R., Ksander, B.R., Merlino, G., Sodhi, A., *et al.* (2014). Hippo-independent activation of YAP by the GNAQ uveal melanoma oncogene through a trio-regulated rho GTPase signaling circuitry. Cancer Cell *25*, 831-845.

Flaherty, K.T., Hodi, F.S., and Fisher, D.E. (2012). From genes to drugs: targeted strategies for melanoma. Nat Rev Cancer *12*, 349-361.

Friend, K., Campbell, Z.T., Cooke, A., Kroll-Conner, P., Wickens, M.P., and Kimble, J. (2012). A conserved PUF-Ago-eEF1A complex attenuates translation elongation. Nat Struct Mol Biol *19*, 176-183.

Futreal, P.A., Coin, L., Marshall, M., Down, T., Hubbard, T., Wooster, R., Rahman, N., and Stratton, M.R. (2004). A census of human cancer genes. Nat Rev Cancer *4*, 177-183.

Goroncy, A.K., Koshiba, S., Tochio, N., Tomizawa, T., Inoue, M., Watanabe, S., Harada, T., Tanaka, A., Ohara, O., Kigawa, T., *et al.* (2010). The NMR solution structures of the five constituent cold-shock domains (CSD) of the human UNR (upstream of N-ras) protein. J Struct Funct Genomics *11*, 181-188.

Hennig, J., Militti, C., Popowicz, G.M., Wang, I., Sonntag, M., Geerlof, A., Gabel, F., Gebauer, F., and Sattler, M. (2014). Structural basis for the assembly of the Sxl-Unr translation regulatory complex. Nature *515*, 287-290.

Hettinger, K., Vikhanskaya, F., Poh, M.K., Lee, M.K., de Belle, I., Zhang, J.T., Reddy, S.A., and Sabapathy, K. (2007). c-Jun promotes cellular survival by suppression of PTEN. Cell Death Differ *14*, 218-229.

Horos, R., Ijspeert, H., Pospisilova, D., Sendtner, R., Andrieu-Soler, C., Taskesen, E., Nieradka, A., Cmejla, R., Sendtner, M., Touw, I.P., *et al.* (2012). Ribosomal deficiencies in Diamond-Blackfan anemia impair translation of transcripts essential for differentiation of murine and human erythroblasts. Blood *119*, 262-272.

Hussey, G.S., Chaudhury, A., Dawson, A.E., Lindner, D.J., Knudsen, C.R., Wilce, M.C., Merrick, W.C., and Howe, P.H. (2011). Identification of an mRNP complex regulating tumorigenesis at the translational elongation step. Mol Cell *41*, 419-431.

Ingolia, N.T., Ghaemmaghami, S., Newman, J.R., and Weissman, J.S. (2009). Genome-wide analysis in vivo of translation with nucleotide resolution using ribosome profiling. Science *324*, 218-223.

Kanehisa, M., and Goto, S. (2000). KEGG: kyoto encyclopedia of genes and genomes. Nucleic Acids Res *28*, 27-30.

Kanehisa, M., Goto, S., Sato, Y., Kawashima, M., Furumichi, M., and Tanabe, M. (2014). Data, information, knowledge and principle: back to metabolism in KEGG. Nucleic Acids Res *42*, D199-205.

Kappelmann, M., Bosserhoff, A., and Kuphal, S. (2014). AP-1/c-Jun transcription factors: regulation and function in malignant melanoma. Eur J Cell Biol *93*, 76-81.

Konig, J., Zarnack, K., Rot, G., Curk, T., Kayikci, M., Zupan, B., Turner, D.J., Luscombe, N.M., and Ule, J. (2011). iCLIP--transcriptome-wide mapping of protein-RNA interactions with individual nucleotide resolution. J Vis Exp.

Krauthammer, M., Kong, Y., Ha, B.H., Evans, P., Bacchiocchi, A., McCusker, J.P., Cheng, E., Davis, M.J., Goh, G., Choi, M., *et al.* (2012). Exome sequencing identifies recurrent somatic RAC1 mutations in melanoma. Nat Genet *44*, 1006-1014.

Liu, B., Han, Y., and Qian, S.B. (2013). Cotranslational response to proteotoxic stress by elongation pausing of ribosomes. Mol Cell *49*, 453-463.

Mihailovic, M., Wurth, L., Zambelli, F., Abaza, I., Militti, C., Mancuso, F.M., Roma, G., Pavesi, G., and Gebauer, F. (2012). Widespread generation of alternative UTRs contributes to sex-specific RNA binding by UNR. RNA *18*, 53-64.

Mihailovich, M., Militti, C., Gabaldon, T., and Gebauer, F. (2010). Eukaryotic cold shock domain proteins: highly versatile regulators of gene expression. Bioessays *32*, 109-118.

Militti, C., Maenner, S., Becker, P.B., and Gebauer, F. (2014). UNR facilitates the interaction of MLE with the lncRNA roX2 during Drosophila dosage compensation. Nat Commun *5*, 4762.

Mitchell, S.A., Spriggs, K.A., Coldwell, M.J., Jackson, R.J., and Willis, A.E. (2003). The Apaf-1 internal ribosome entry segment attains the correct structural conformation for function via interactions with PTB and unr. Mol Cell *11*, 757-771.

Morris, A.R., Mukherjee, N., and Keene, J.D. (2010). Systematic analysis of posttranscriptional gene expression. Wiley Interdiscip Rev Syst Biol Med *2*, 162-180.

Novak, M., Leonard, M.K., Yang, X.H., Kowluru, A., Belkin, A.M., and Kaetzel, D.M. (2015). Metastasis suppressor NME1 regulates melanoma cell morphology, self-adhesion and motility via induction of fibronectin expression. Exp Dermatol *24*, 455-461.

Patel, G.P., Ma, S., and Bag, J. (2005). The autoregulatory translational control element of poly(A)-binding protein mRNA forms a heteromeric ribonucleoprotein complex. Nucleic Acids Res *33*, 7074-7089.

Qian, B.Z., Li, J., Zhang, H., Kitamura, T., Zhang, J., Campion, L.R., Kaiser, E.A., Snyder, L.A., and Pollard, J.W. (2011). CCL2 recruits inflammatory monocytes to facilitate breast-tumour metastasis. Nature *475*, 222-225.

Ridgway, L.D., Wetzel, M.D., and Marchetti, D. (2010). Modulation of GEF-H1 induced signaling by heparanase in brain metastatic melanoma cells. J Cell Biochem *111*, 1299-1309.

Satelli, A., and Li, S. (2011). Vimentin in cancer and its potential as a molecular target for cancer therapy. Cell Mol Life Sci *68*, 3033-3046.

Schadendorf, D. et al. (2015). Melanoma. Nat Rev Dis Primers *1*, 15003.

Schepens, B., Tinton, S.A., Bruynooghe, Y., Parthoens, E., Haegman, M., Beyaert, R., and Cornelis, S. (2007). A role for hnRNP C1/C2 and Unr in internal initiation of translation during mitosis. EMBO J *26*, 158-169.

Shalgi, R., Hurt, J.A., Krykbaeva, I., Taipale, M., Lindquist, S., and Burge, C.B. (2013). Widespread regulation of translation by elongation pausing in heat shock. Mol Cell *49*, 439-452.

Shannon, P., Markiel, A., Ozier, O., Baliga, N.S., Wang, J.T., Ramage, D., Amin, N., Schwikowski, B., and Ideker, T. (2003). Cytoscape: a software environment for integrated models of biomolecular interaction networks. Genome Res *13*, 2498-2504.

Shao, H., Kirkwood, J.M., and Wells, A. (2015). Tenascin-C Signaling in melanoma. Cell adhesion & migration *9*, 125-130.

Sonenberg, N., and Hinnebusch, A.G. (2009). Regulation of translation initiation in eukaryotes: mechanisms and biological targets. Cell *136*, 731-745.

Thompson, J.F., Shaw, H.M., Hersey, P., and Scolyer, R.A. (2004). The history and future of melanoma staging. J Surg Oncol *86*, 224-235.

Tinton, S.A., Schepens, B., Bruynooghe, Y., Beyaert, R., and Cornelis, S. (2005). Regulation of the cell-cycle-dependent internal ribosome entry site of the PITSLRE protein kinase: roles of Unr (upstream of N-ras) protein and phosphorylated translation initiation factor eIF-2alpha. Biochem J *385*, 155-163.

Triqueneaux, G., Velten, M., Franzon, P., Dautry, F., and Jacquemin-Sablon, H. (1999). RNA binding specificity of Unr, a protein with five cold shock domains. Nucleic Acids Res *27*, 1926-1934.

Vaque, J.P., Dorsam, R.T., Feng, X., Iglesias-Bartolome, R., Forsthoefel, D.J., Chen, Q., Debant, A., Seeger, M.A., Ksander, B.R., Teramoto, H., et al. (2013). A genome-wide RNAi screen reveals a Trio-regulated Rho GTPase circuitry transducing mitogenic signals initiated by G protein-coupled receptors. Mol Cell *49*, 94-108.

Wan, Y., Qu, K., Zhang, Q.C., Flynn, R.A., Manor, O., Ouyang, Z., Zhang, J., Spitale, R.C., Snyder, M.P., Segal, E., *et al.* (2014). Landscape and variation of RNA secondary structure across the human transcriptome. Nature *505*, 706-709.

Wolter, S., Doerrie, A., Weber, A., Schneider, H., Hoffmann, E., von der Ohe, J., Bakiri, L., Wagner, E.F., Resch, K., and Kracht, M. (2008). c-Jun controls histone

modifications, NF-kappaB recruitment, and RNA polymerase II function to activate the ccl2 gene. Mol Cell Biol *28*, 4407-4423.

Wurth, L., and Gebauer, F. (2015). RNA-binding proteins, multifaceted translational regulators in cancer. Biochim Biophys Acta *1849*, 881-886.

Figure legends

Figure 1. UNR is upregulated in melanoma

(A) Western blot of UNR in melanoma cell lines and non tumoral melanocytes. Tubulin is shown as a loading control. A quantification of the UNR signal corrected for tubulin is shown at the bottom. A red line has been drawn at the levels observed in melanocytes to facilitate inspection. (B) UNR expression in malignant and benign patient tumor samples monitored by immunohistochemistry (IHC). The same commercial anti-UNR antibody used in (A) was employed for IHC. IHC scoring was performed blind, prior to association with clinical data. Left and right scale bars represent 200 µM and 20 µM, respectively. See also Figure S1.

Figure 2. UNR promotes melanoma invasion and metastasis

(A) SK-Mel-103 melanoma cells were stably transduced with a lentiviral doxycycline inducible shRNA. Western blot (left), cumulative (middle) and standard (right) growth curves. Grey, shControl; black, shUNR. Error bars represent the standard error (SEM) of triplicate experiments. The insets show typical bright field microscopy views of shControl and shUNR cells. (B) Colony formation assay in cells as in A. One representative whole well from a 6-well plate is shown per condition (n= 6). (C) Soft agar assays of cells expressing shUNR or shControl, and GFP or RNAi-resistant

UNR-Flag. One representative whole well from a 12-well plate is shown per condition (n= 10). (D) Analysis of anoikis. Cells were grown in ultra-low attachment plates and growth was documented by bright field microscopy. The scale bar represents 500 µM (n= 4). (E) The mean speed of migration of SK-Mel-103 cells embedded into collagen was analyzed by time lapse microscopy. The number of cells analyzed from 3 different experiments is indicated (n). Center lines show the medians, box limits indicate the 25th and 75th percentiles as determined by R software, whiskers extend 1.5 times the interquartile range from the 25th and 75th percentiles, and outliers are represented by dots. (F) Invasion assay of cell spheres embedded in matrigel monitored by bright field microscopy. The scale bar represents 500 µM. The invasion area is shown in red (n= 4). (G) shControl or shUNR cells were injected subcutaneously into nude mice. Tumors were resected and weighted (n= 18 shControl, n= 16 shControl+dox, n= 18 shUNR, n= 19 shUNR+dox). Error bars represent the standard error (SEM). (H) Melanoma shUNR and shControl cells expressing a luciferase reporter were injected into the tail vein of nude mice and metastasis to the lung was followed (n= 5 mice per experimental genotype). Lung architecture was analyzed by H&E staining. The scale bar represents 50 µM. (I) Metastatic SK-Mel-103 cells expressing shUNR or shControl (upper panel, n= 6) or non-metastatic UACC-257 cells expressing UNR or control GFP (lower panel, n= 5) were injected subcutaneously into the flanks of nude mice. All cells contained a luciferase reporter. Tumors were allowed to grow until they reached 1500 mm^3, at which moment the sentinel (inguinal, I) and distal (axillary, A; brachial, B) lymph nodes at both sides of the animal were extracted and analyzed for the presence of metastatic cells. Representative images are shown at the left, where red circles mark positive lymph nodes for metastasis. A quantification is shown at the right. Center

lines show the mean value and side bars represent 1 SD as calculated by Graphpad software. The number of LN metastasis in each animal is represented by dots. Significance was assessed by Student's t-Test (p value * ≤0.05, **≤0.01, ***≤0.001). See also Figure S2 and Movies S1 and S2.

Figure 3. Identification of UNR RNA targets by iCLIP-Seq

(A) Experimental strategy to unravel the molecular mechanisms underlying the role of UNR in melanoma. (B) iCLIP controls. Left, Western blot of anti-UNR (αUNR) and control (IgG) immunoprecipitates with our αUNR antibody; i, input. Asterisks denote non-specific bands. Right, UNR-RNA complexes used in iCLIP (see text for details). (C) Venn diagram depicting the number of targets identified in 2 independent iCLIP experiments. (D) UNR iCLIP profiles for *PABPC1* and *CSDE1/UNR* mRNAs. (E) Scatterplot showing the correlation between UNR binding (iCLIP tag enrichment) and UNR target levels (mRNA abundance). Orange and green dots depict coding and non-coding RNAs with called UNR peaks, respectively. Blue dots depict RNAs with no detectable UNR binding. (F) UNR binding motif. (G) UNR iCLIP tag density in different transcript regions. (H) PARS analysis of the structure of UNR targets (brown) compared to all transcripts (black). (I) Metagene analysis of UNR binding along the mRNA. Tag counts are normalized for coverage within the experiment. See also Figure S3 and Tables S1, S2, S3 and S6.

Figure 4. UNR targets regulated at the steady state level

(A) Scatterplot showing the correlation between iCLIP tag enrichment and mRNA abundance change between shUNR and shControl cells. Orange points denote UNR targets. (B) Left, Venn diagram illustrating the overlap of genes regulated at the

steady state level and iCLIP targets. Right, Heatmaps of changes in RNA levels upon UNR depletion for all genes and iCLIP targets. (C) Gene Ontology analysis of all genes changing at the steady state level. Similar results were obtained for iCLIP targets. (D) Validation of transcript level changes by RT-qPCR. *GUSB* and *PSMB4* were used as negative controls. RNA-Seq data is included as comparison. Error bars represent the standard error (SEM) of at least 3 experiments. (E) Metagene analysis of UNR binding in regulated transcripts. See also Figure S4 and Tables S1, S4 and S6.

Figure 5. UNR targets regulated at the translation level

(A) Venn diagram depicting the overlaps of the analysis performed in this study. (B) Gene Ontology analysis of genes changing at the translation level upon UNR depletion. Similar results were obtained for direct UNR targets. (C) Summary of all changes detected upon UNR depletion (see text for details). Black, mRNAs showing ribosome distribution changes; orange, UNR targets. (D) Metagene analysis of UNR position along the mRNA in transcripts regulated at the level of ribosome distribution or RPF. (E) Top, ribosome distribution changes on *VIM* and *RAC1* mRNAs upon UNR depletion; p values for the significance of differences in distribution are shown (Smirnov-Kolmogorov, two-sample, two-sided test). Bottom, effect of UNR depletion on VIM and RAC1 protein levels. (F) Ribosome run-off assays. Newly synthesized VIM, Tubulin and Vinculin were monitored in shControl and shUNR cells by metabolic labeling using amino acids susceptible to click chemistry. A scheme of the labeling protocol is shown at the top. Translation initiation was inhibited with Harringtonine for 10 min, and samples were taken at 0 or 10 min after Harringtonine inhibition. Newly synthesized proteins were labeled with biotin using click-chemistry, selected with streptavidin beads, and resolved by SDS-PAGE followed by Western

blot. Proteins were quantified and plotted relative to the levels at t= 0. Two independent experiments (EXP1, EXP2) were performed. (G) Top, iCLIP profile of UNR binding to *VIM* mRNA. Bottom, Firefly luciferase reporter mRNAs were transfected into shControl and shUNR melanoma cells treated or not with doxycycline. Luciferase values were corrected for Luciferase mRNA levels, and represented as the efficiency of translation relative to shControl cells. Error bars represent the standard error (SEM) of triplicate experiments. Significance was assessed by Student's t-Test. See also Figure S5 and Tables S1, S5 and S6.

Figure 6. UNR regulates a network of genes relevant for melanoma progression

(A) Network analysis of UNR targets. Yellow, melanoma relevant genes. Targets regulated by UNR at the steady state (violet) or translation (green) levels that intersect with melanoma genes are shown. Connections represent interactions, broadly defined as metabolic catalysis, co-regulation, protein interaction, same complex, reaction with and state change (i.e. post-translational modification or change in subcellular localization). Boxes enclose RNA regulons discussed in the text. Genes studied in more detail in this report are shadowed. (B) UNR was either depleted or over-expressed and the levels of protein products were analyzed by Western blot. Depletion of UNR was induced by shRNA expression (shU) or by transfecting siRNA pools (siU) for 72 h. Non-specific shRNA (shC) or siRNA pools (siC) were used as controls. Over-expression was achieved using viral expression constructs containing UNR (+U) or GFP (+C) as control. Quantifications from 3 independent experiments is shown at the bottom. Error bars represent the standard deviation (SD). M, melanoma; BC, breast cancer; OC, ovarian cancer.

Figure 7. Regulation of VIM and RAC1 by UNR modulates cancerous traits.

(A) Colony forming capacity of UNR depleted cells after over-expression of LOXL2 (n=10). (B) Colony forming capacity of UNR depleted cells after over-expression of VIM and RAC1 (n=7-10). Box plots are defined as in the legend of Figure 2E. Significance was verified by Student's t-test. ns, not significant. See also Table S7.

Figure 1

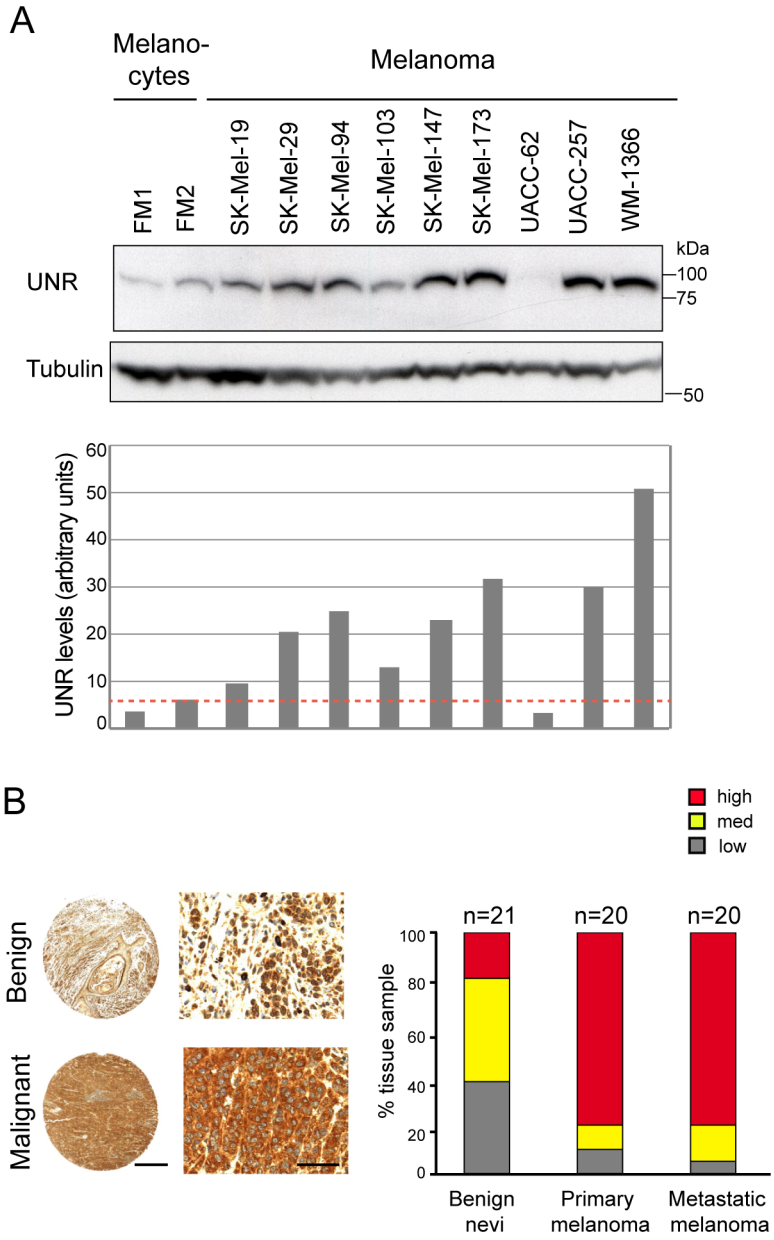
A
Melano-cytes
Melanoma
FM1
FM2
SK-Mel-19
SK-Mel-29
SK-Mel-94
SK-Mel-103
SK-Mel-147
SK-Mel-173
UACC-62
UACC-257
WM-1366
kDa
UNR
100
75
Tubulin
50
UNR levels (arbitrary units)
60
50
40
30
20
10
0
B
high
med
low
Benign
Malignant
n=21
n=20
n=20
% tissue sample
100
80
60
40
20
0
Benign nevi
Primary melanoma
Metastatic melanoma

Figure 2

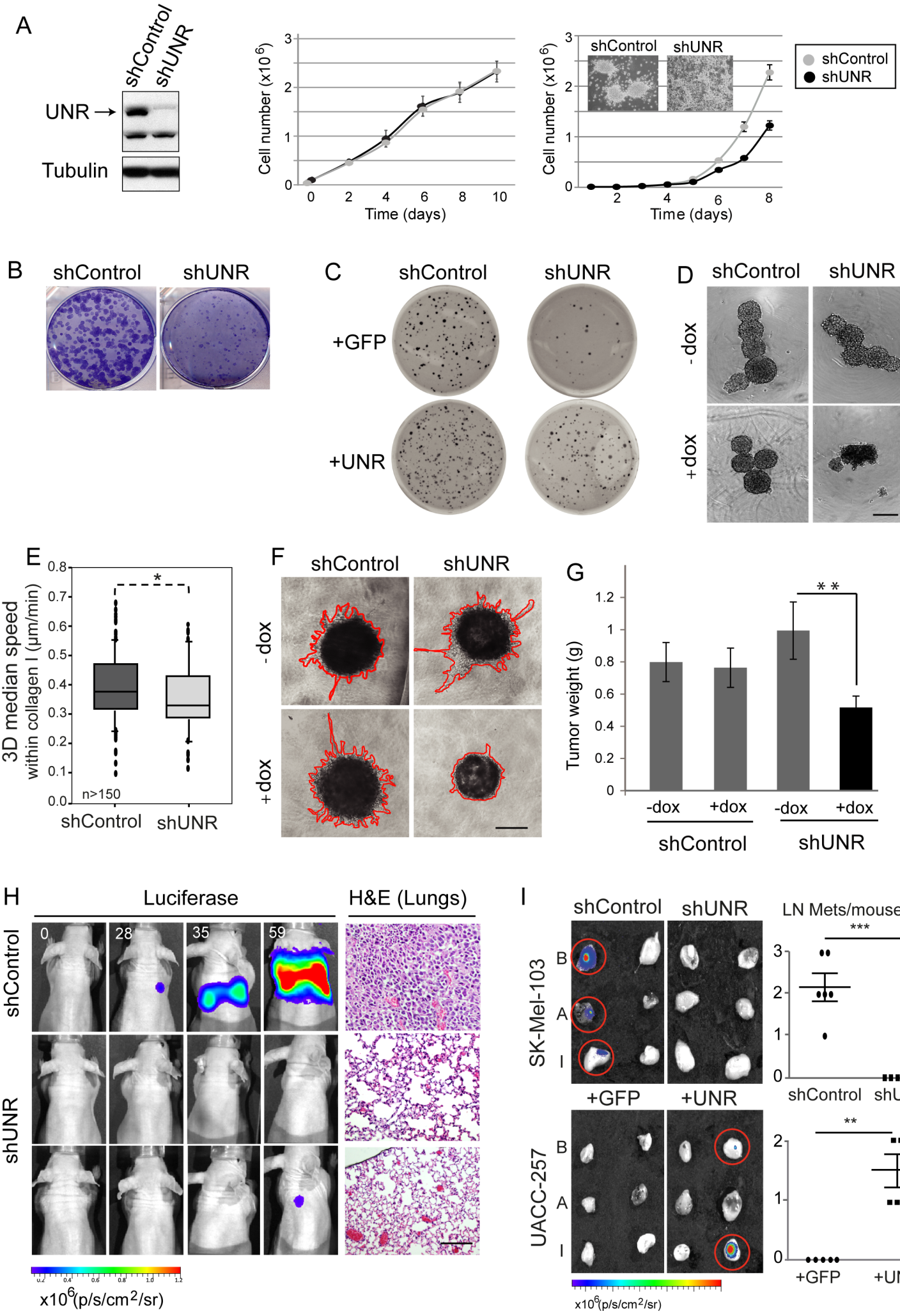
A
shControl
shUNR
UNR
Tubulin
Cell number (x10^6)
Time (days)
shControl
shUNR
B
C
+GFP
+UNR
D
-dox
+dox
E
3D median speed within collagen I (µm/min)
n>150
F
G
Tumor weight (g)
-dox
+dox
H
Luciferase
H&E (Lungs)
0
28
35
59
x10^6(p/s/cm^2/sr)
I
SK-Mel-103
UACC-257
LN Mets/mouse
***
**

Figure 3

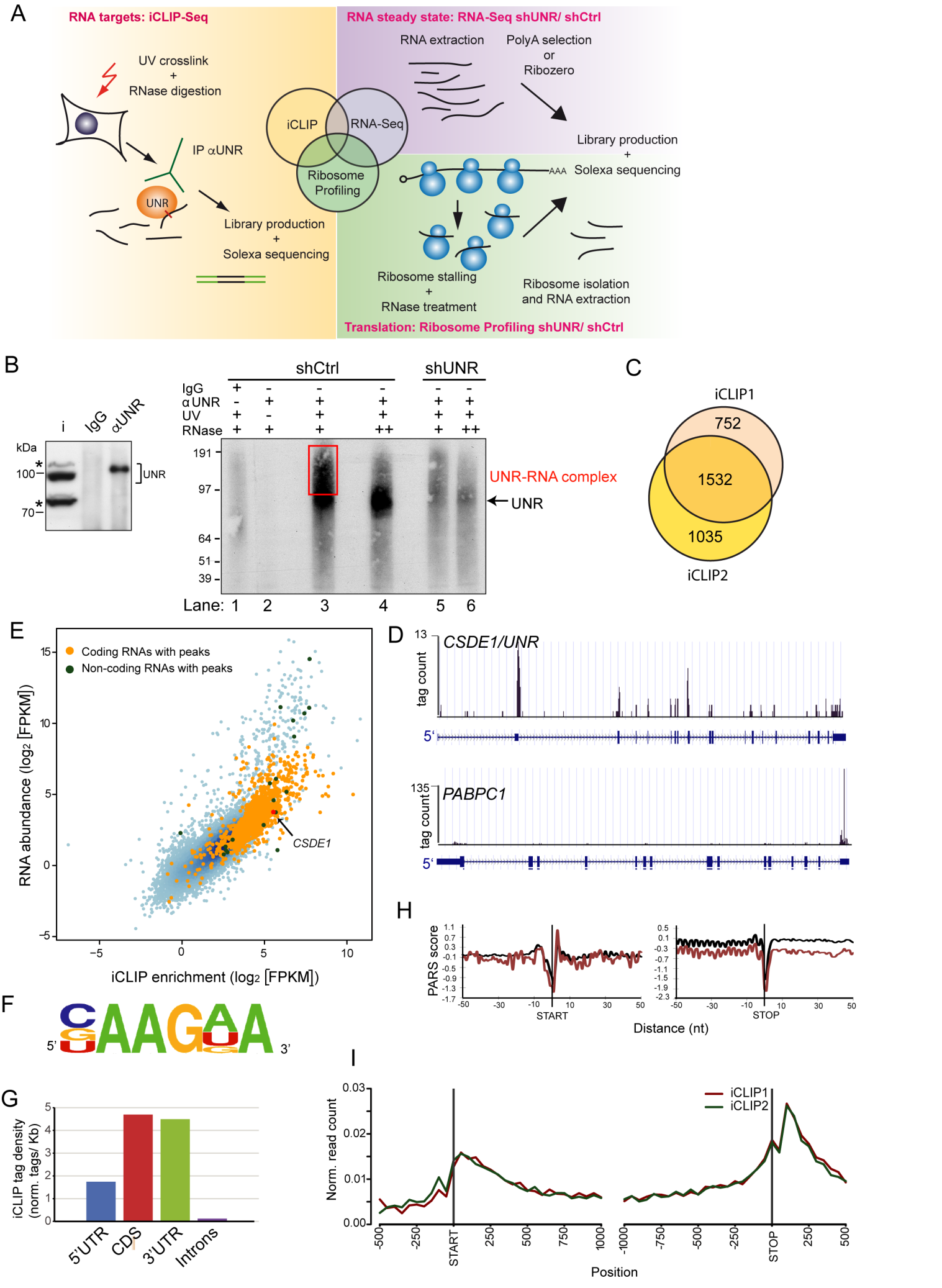
A
RNA targets: iCLIP-Seq
UV crosslink
+
RNase digestion
IP αUNR
UNR
Library production
+
Solexa sequencing
iCLIP
RNA-Seq
Ribosome Profiling
RNA steady state: RNA-Seq shUNR/ shCtrl
RNA extraction
PolyA selection
or
Ribozero
Library production
+
Solexa sequencing
AAA
Ribosome stalling
+
RNase treatment
Ribosome isolation
and RNA extraction
Translation: Ribosome Profiling shUNR/ shCtrl
B
i
IgG
αUNR
kDa
100
70
UNR
shCtrl
shUNR
IgG
αUNR
UV
RNase
191
97
64
51
39
Lane: 1 2 3 4 5 6
UNR-RNA complex
UNR
C
iCLIP1
752
1532
1035
iCLIP2
E
Coding RNAs with peaks
Non-coding RNAs with peaks
RNA abundance (log2 [FPKM])
iCLIP enrichment (log2 [FPKM])
CSDE1
D
CSDE1/UNR
tag count
5'
135
PABPC1
H
PARS score
START
STOP
Distance (nt)
F
5'
3'
G
iCLIP tag density
(norm. tags/ Kb)
5'UTR
CDS
3'UTR
Introns
I
Norm. read count
iCLIP1
iCLIP2
START
STOP
Position

Figure 4

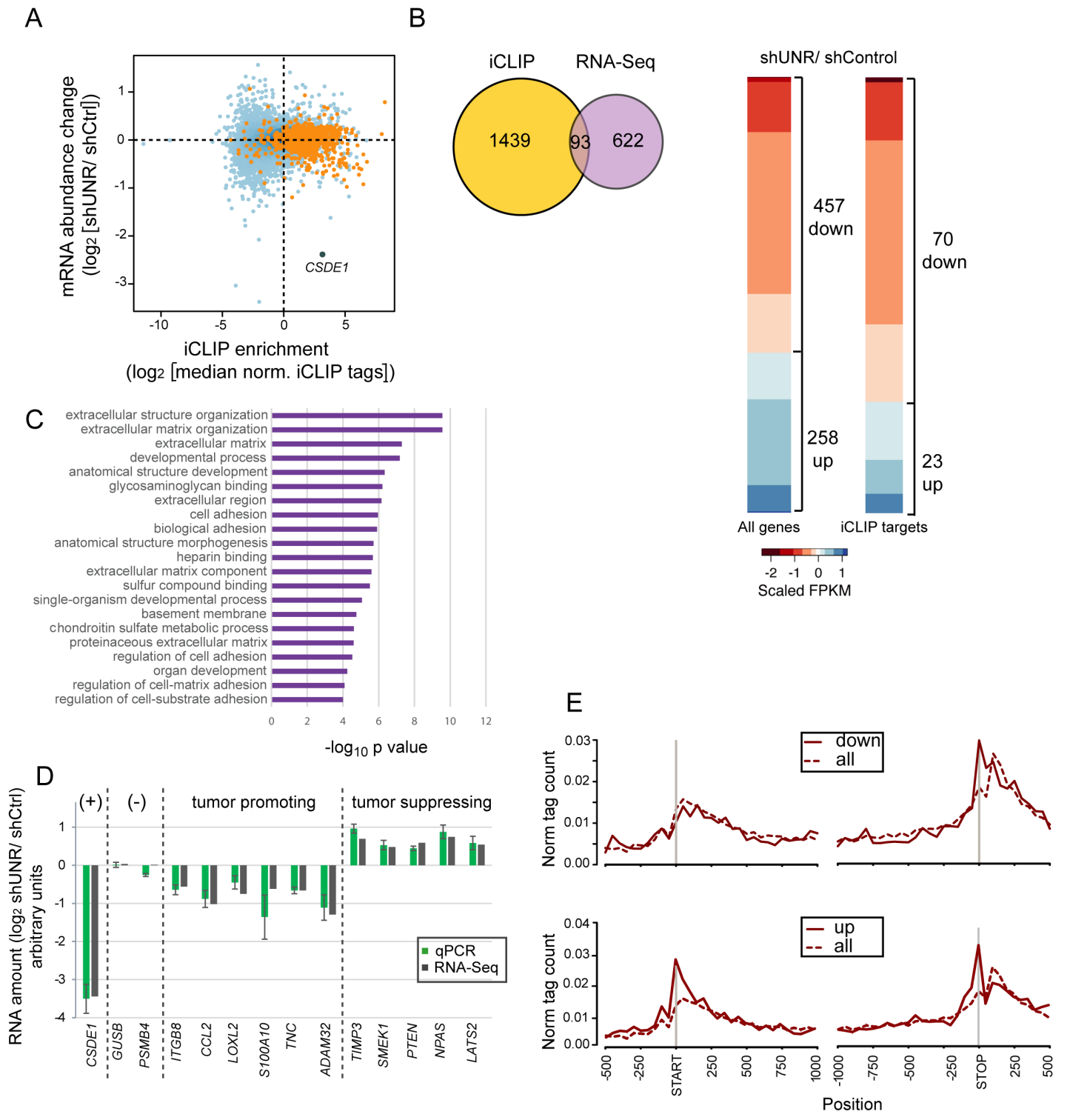
A
mRNA abundance change
(log2 [shUNR/ shCtrl])
iCLIP enrichment
(log2 [median norm. iCLIP tags])
CSDE1
B
iCLIP
RNA-Seq
1439
93
622
shUNR/ shControl
457
down
258
up
70
down
23
up
All genes
iCLIP targets
-2 -1 0 1
Scaled FPKM
C
extracellular structure organization
extracellular matrix organization
extracellular matrix
developmental process
anatomical structure development
glycosaminoglycan binding
extracellular region
cell adhesion
biological adhesion
anatomical structure morphogenesis
heparin binding
extracellular matrix component
sulfur compound binding
single-organism developmental process
basement membrane
chondroitin sulfate metabolic process
proteinaceous extracellular matrix
regulation of cell adhesion
organ development
regulation of cell-matrix adhesion
regulation of cell-substrate adhesion
-log10 p value
D
(+)
(-)
tumor promoting
tumor suppressing
RNA amount (log2 shUNR/ shCtrl)
arbitrary units
qPCR
RNA-Seq
CSDE1
GUSB
PSMB4
ITGB8
CCL2
LOXL2
S100A10
TNC
ADAM32
TIMP3
SMEK1
PTEN
NPAS
LATS2
E
down
all
up
all
Norm tag count
START
STOP
Position

Figure 5

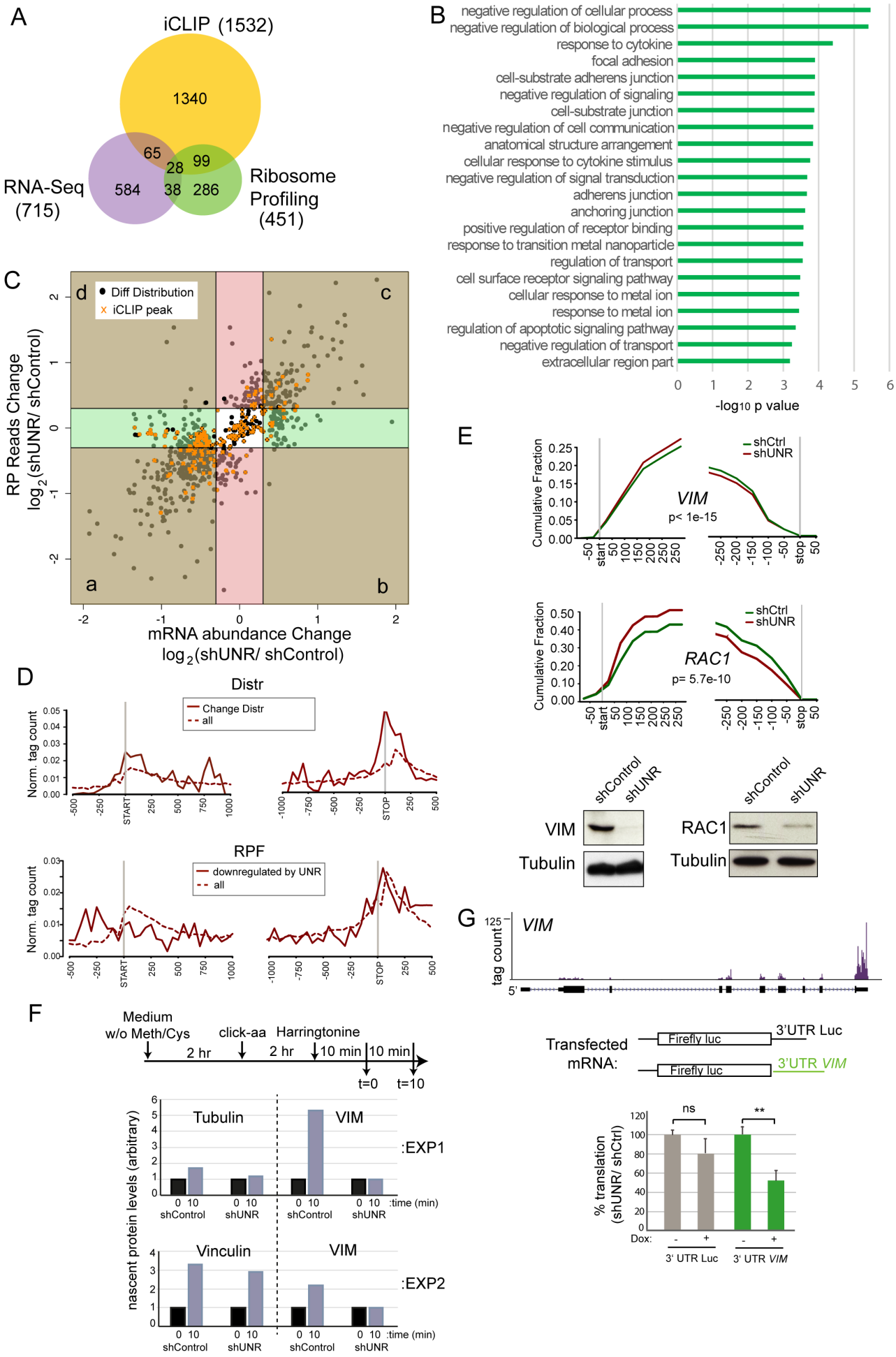
A
iCLIP (1532)
1340
65
28
99
RNA-Seq
(715)
584
38
286
Ribosome
Profiling
(451)
B
negative regulation of cellular process
negative regulation of biological process
response to cytokine
focal adhesion
cell-substrate adherens junction
negative regulation of signaling
cell-substrate junction
negative regulation of cell communication
anatomical structure arrangement
cellular response to cytokine stimulus
negative regulation of signal transduction
adherens junction
anchoring junction
positive regulation of receptor binding
response to transition metal nanoparticle
regulation of transport
cell surface receptor signaling pathway
cellular response to metal ion
response to metal ion
regulation of apoptotic signaling pathway
negative regulation of transport
extracellular region part
-log10 p value
C
Diff Distribution
iCLIP peak
RP Reads Change
log2(shUNR/ shControl)
mRNA abundance Change
log2(shUNR/ shControl)
D
Distr
Change Distr
all
Norm. tag count
RPF
downregulated by UNR
all
E
shCtrl
shUNR
Cumulative Fraction
VIM
p< 1e-15
RAC1
p= 5.7e-10
shControl
shUNR
VIM
Tubulin
RAC1
Tubulin
F
Medium
w/o Meth/Cys
click-aa
Harringtonine
2 hr
2 hr
10 min
10 min
t=0
t=10
Tubulin
VIM
:EXP1
Vinculin
VIM
:EXP2
nascent protein levels (arbitrary)
shControl
shUNR
:time (min)
G
VIM
tag count
5'
Transfected
mRNA:
Firefly luc
3'UTR Luc
Firefly luc
3'UTR VIM
% translation
(shUNR/ shCtrl)
ns
**
Dox:
3' UTR Luc
3' UTR VIM

Figure 6

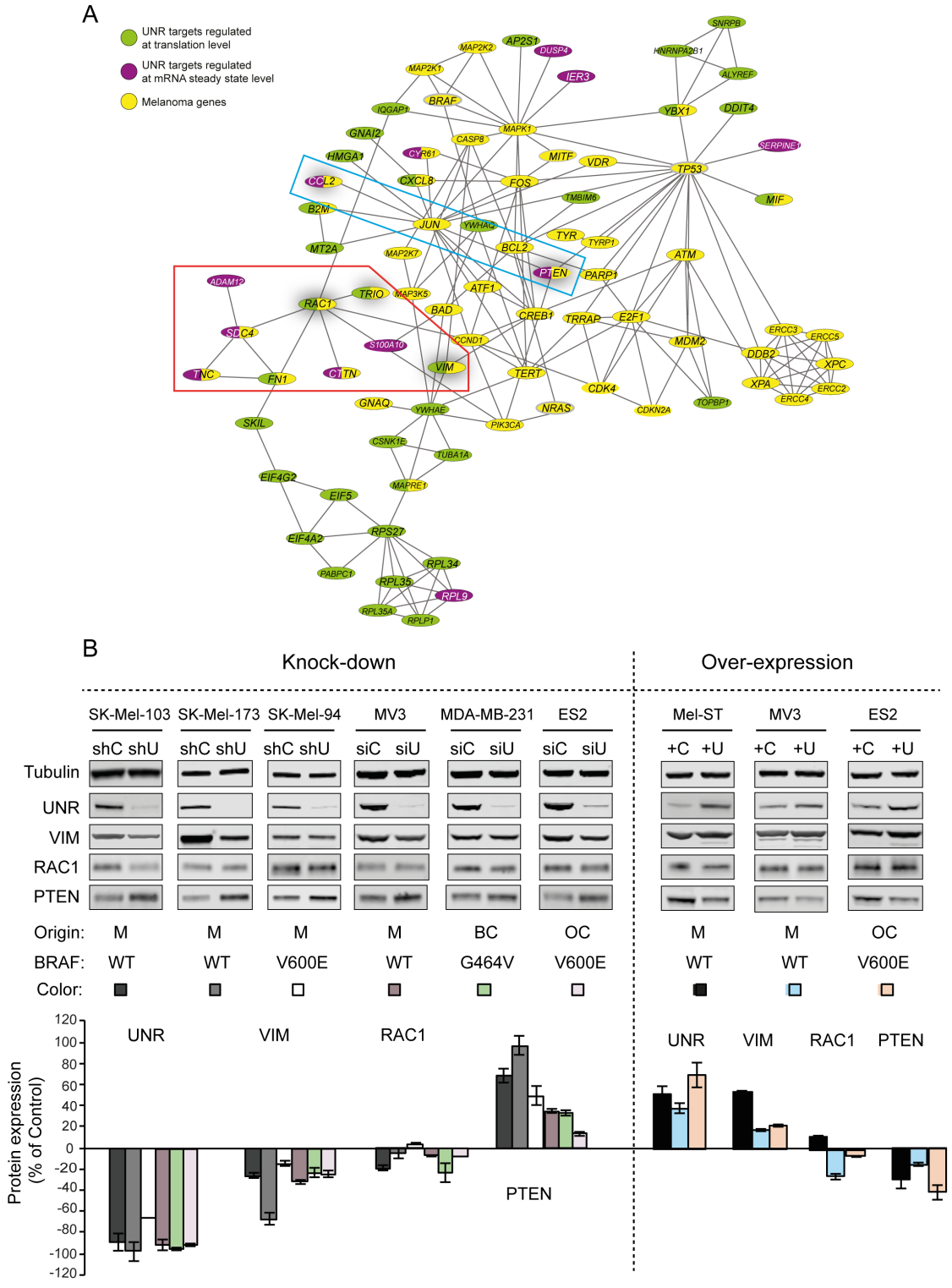
A
UNR targets regulated at translation level
UNR targets regulated at mRNA steady state level
Melanoma genes
SNRPB
HNRNPA2B1
ALYREF
YBX1
DDIT4
SERPINE1
MIF
TP53
VDR
MITF
FOS
TMBIM6
CXCL8
CCL2
CYR61
HMGA1
CASP8
MAPK1
IER3
DUSP4
AP2S1
MAP2K2
MAP2K1
BRAF
IQGAP1
GNAI2
B2M
JUN
YWHAC
MT2A
MAP2K7
TYR
TYRP1
BCL2
PTEN
PARP1
ATM
ADAM12
TRIO
RAC1
MAP3K5
ATF1
BAD
CREB1
TRRAP
E2F1
MDM2
ERCC3
ERCC5
DDB2
XPC
XPA
ERCC2
ERCC4
TOPBP1
CDKN2A
CDK4
TERT
VIM
S100A10
CCND1
SLC4
TNC
FN1
CTTN
GNAQ
YWHAE
NRAS
PIK3CA
SKIL
CSNK1E
TUBA1A
EIF4G2
EIF5
MAPRE1
EIF4A2
RPS27
PABPC1
RPL34
RPL35
RPL9
RPL35A
RPLP1
B
Knock-down
Over-expression
SK-Mel-103
SK-Mel-173
SK-Mel-94
MV3
MDA-MB-231
ES2
Mel-ST
MV3
ES2
shC shU
siC siU
+C +U
Tubulin
UNR
VIM
RAC1
PTEN
Origin: M M M M BC OC M M OC
BRAF: WT WT V600E WT G464V V600E WT WT V600E
Color:
Protein expression (% of Control)
120
100
80
60
40
20
0
-20
-40
-60
-80
-100
-120
UNR
VIM
RAC1
PTEN

Figure 7

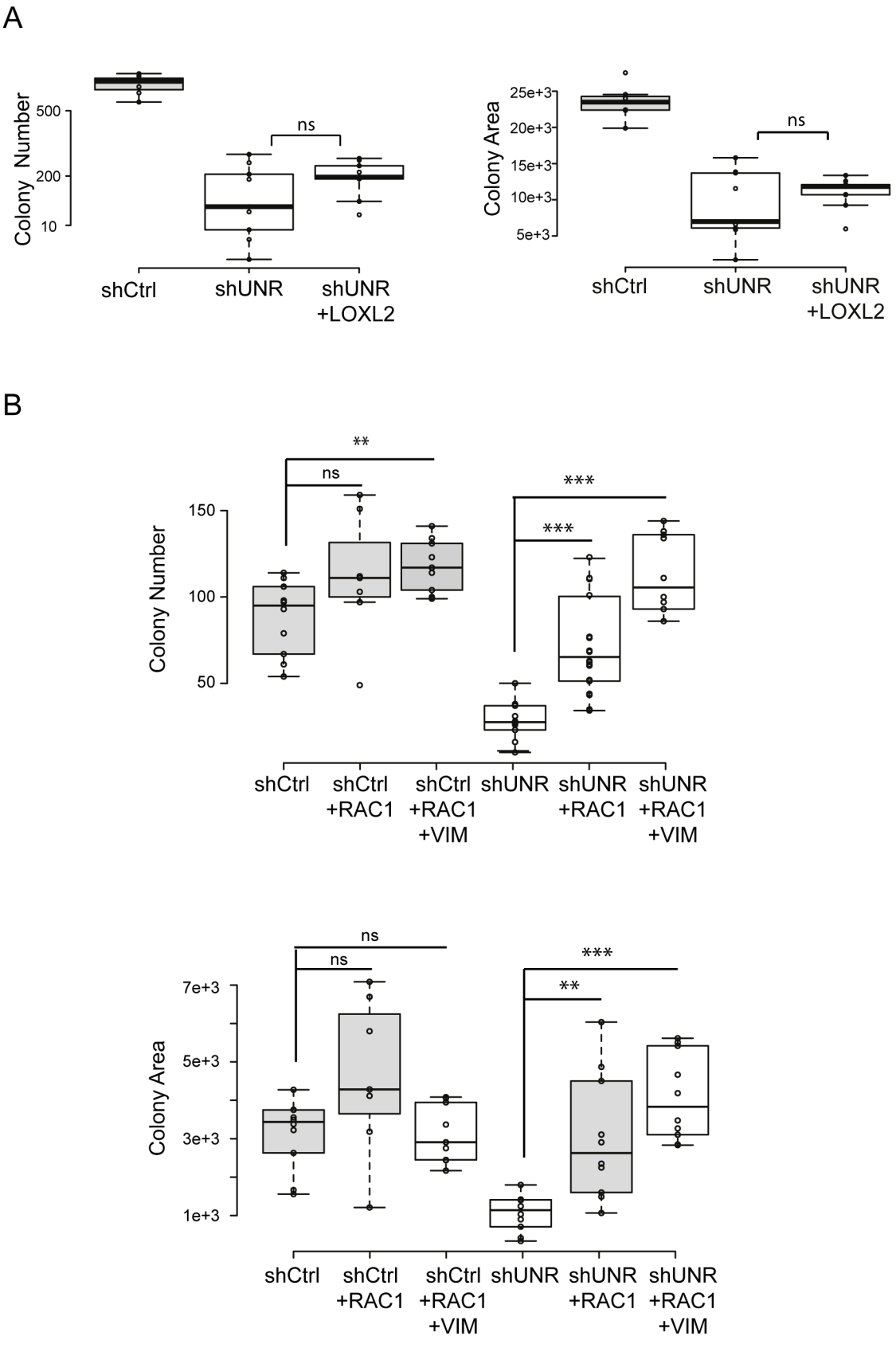
A
Colony Number
500
200
10
ns
shCtrl
shUNR
shUNR +LOXL2
Colony Area
25e+3
20e+3
15e+3
10e+3
5e+3
ns
shCtrl
shUNR
shUNR +LOXL2
B
Colony Number
150
100
50
**
ns
***
***
shCtrl
shCtrl +RAC1
shCtrl +RAC1 +VIM
shUNR
shUNR +RAC1
shUNR +RAC1 +VIM
Colony Area
7e+3
5e+3
3e+3
1e+3
ns
ns
***
**
shCtrl
shCtrl +RAC1
shCtrl +RAC1 +VIM
shUNR
shUNR +RAC1
shUNR +RAC1 +VIM

SUPPLEMENTAL DATA

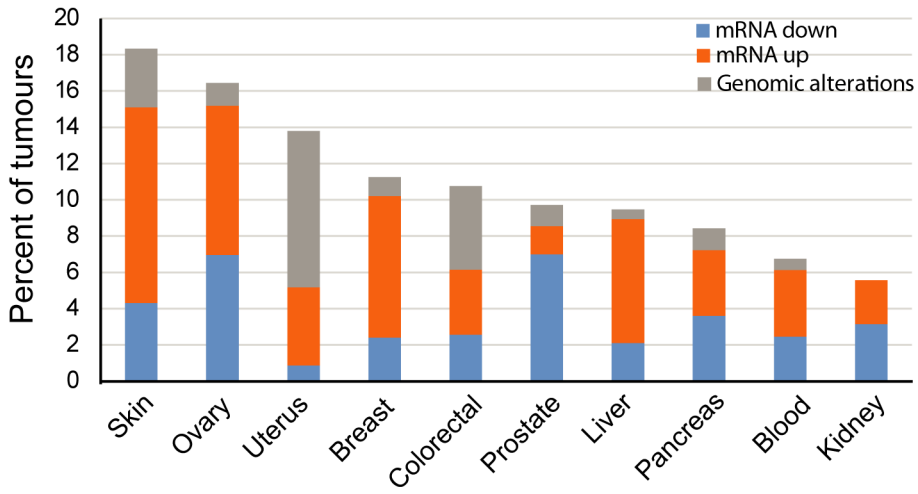

Figure S1. UNR Alterations Across Tumors (Related to Figure 1)
Genomic alterations (mutations, deletions and amplifications) and *CSDE1/UNR* transcript levels were scored in different tumors using data from the TCGA database (http://cancergenome.nih.gov/) using cBio-Portal for Cancer Genomics (Cerami et al., 2012; Gao et al., 2013). Skin, Cutaneous Melanoma (n= 278); Ovary, Ovarian Serous Cystadenocarcinoma (n= 158); Uterus, Uterine Corpus Endometrioid Carcinoma (n= 232); Breast, Breast Invasive Carcinoma (n= 959); Colorectal, Colorectal Adenocarcinoma (n= 195); Prostate, Prostate Adenocarcinoma (n= 257); Liver, Hepatocellular Carcinoma (n= 190); Pancreas, Pancreatic Adenocarcinoma (n= 83); Blood, Acute Myeloid Leukemia (n= 163); Kidney, Renal Clear Cell Carcinoma (n= 413).

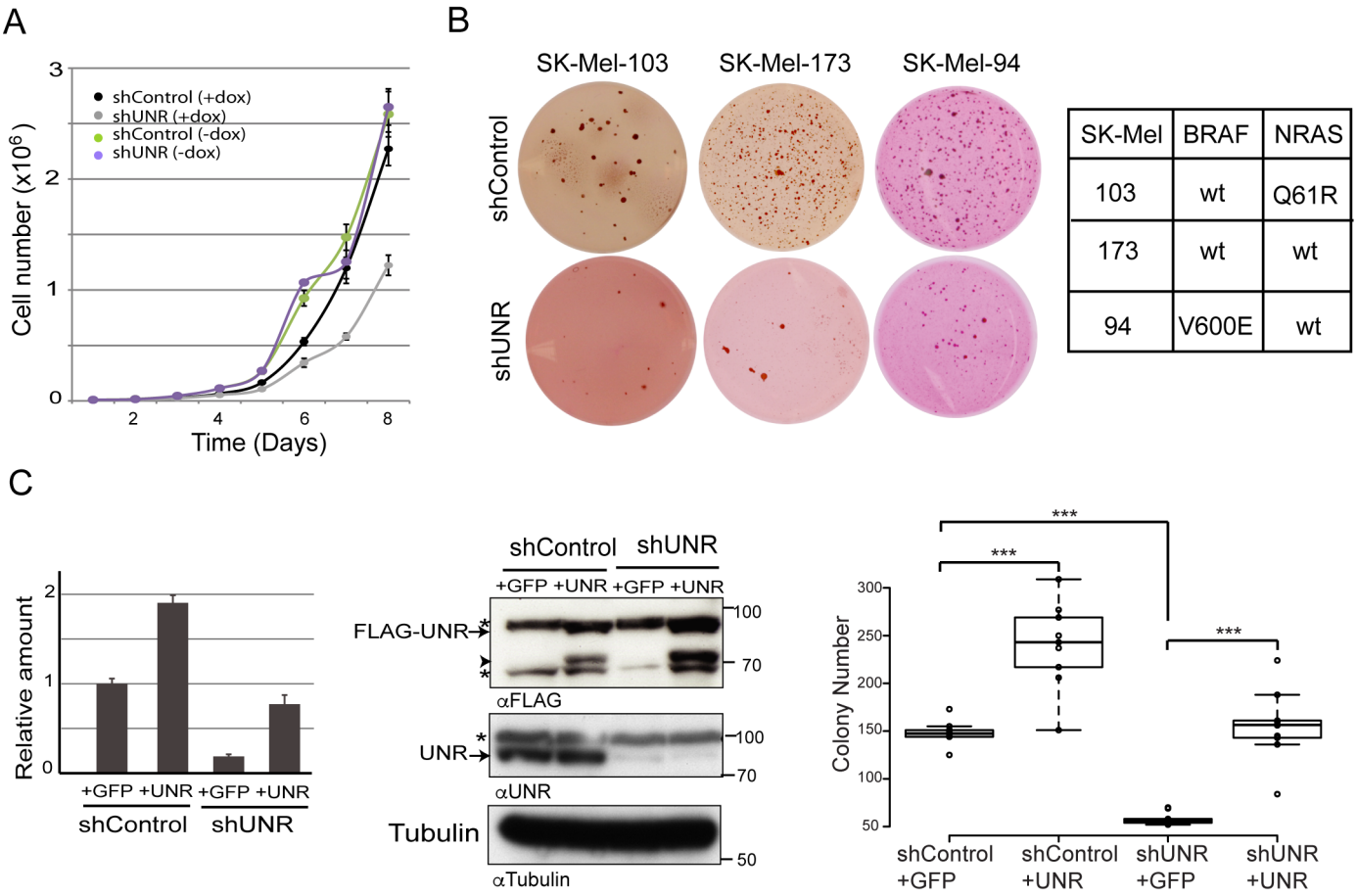
A
Cell number (x10^6)
Time (Days)
shControl (+dox)
shUNR (+dox)
shControl (-dox)
shUNR (-dox)
B
SK-Mel-103
SK-Mel-173
SK-Mel-94
shControl
shUNR
SK-Mel | BRAF | NRAS
103 | wt | Q61R
173 | wt | wt
94 | V600E | wt
C
Relative amount
+GFP +UNR +GFP +UNR
shControl shUNR
shControl shUNR
+GFP +UNR +GFP +UNR
FLAG-UNR
αFLAG
UNR
αUNR
Tubulin
αTubulin
Colony Number
shControl +GFP
shControl +UNR
shUNR +GFP
shUNR +UNR
D
Spheroid number
dox:
shControl shUNR
Spheroid area (µm)²
E
rel. spheroid viability
rel. caspase 3/7 activity (normed to viability)
F
Invasion index (% of control)
Spheroid area (µm)²
G
3D median speed within collagen I (µm/min)
n>150
+GFP +UNR
invasion index (% control)

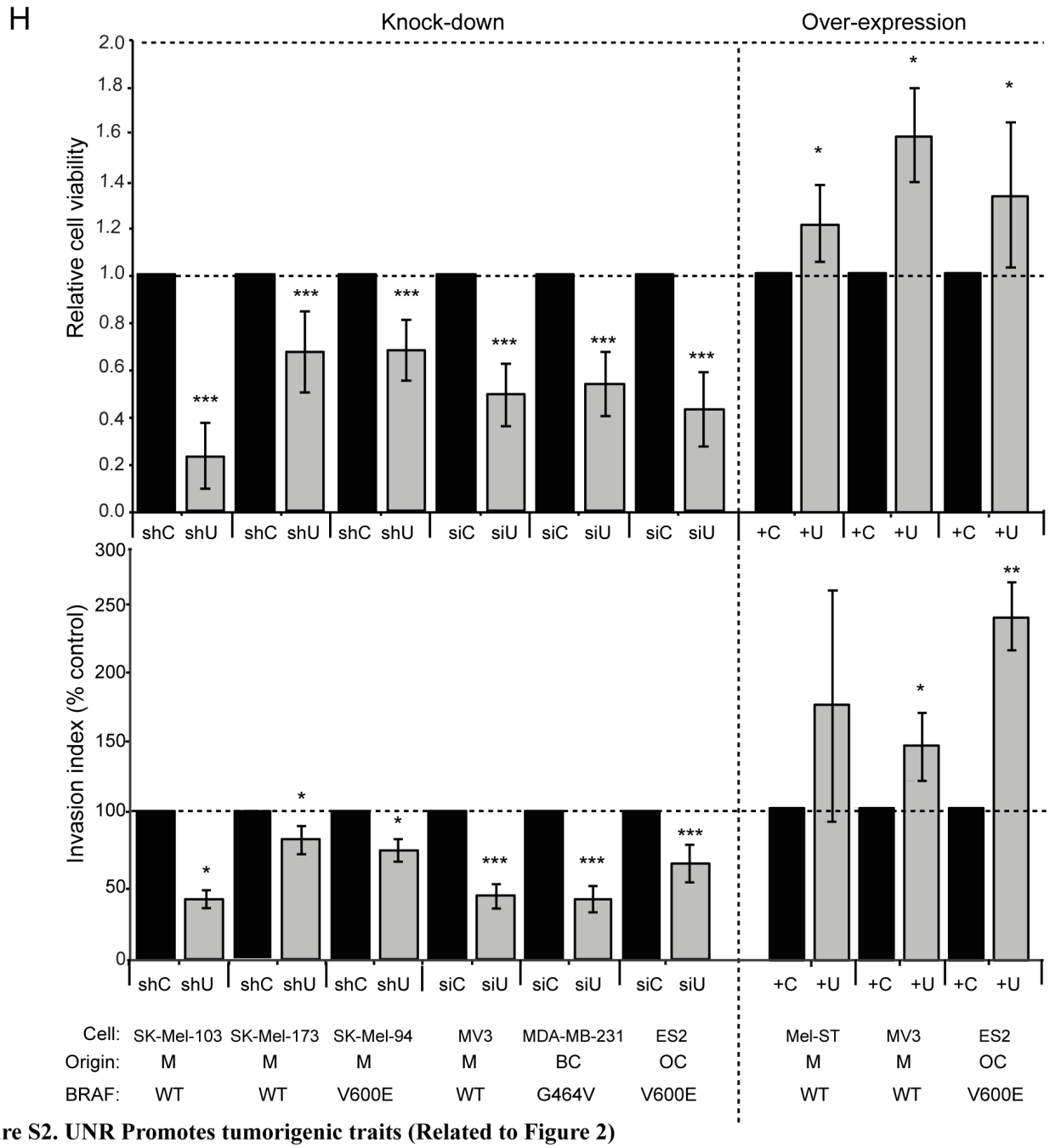

Figure S2. UNR Promotes tumorigenic traits (Related to Figure 2)

(A) Growth of SK-Mel-103 cells expressing or not shControl or shUNR. shRNA expression was induced with doxycycline (n= 3).

(B) Soft agar colony formation assays of melanoma cells with different genetic backgrounds (see table on the right) expressing or not shControl or shUNR: SK-Mel-103 (n=10), SK-Mel-173 (n=5), SK-Mel-94 (n=10). One representative whole well from a 12-well plate is shown per condition.

(C) Assessment of UNR expression in soft agar recovery assays. The levels of *CSDE1/UNR* mRNA (left) or protein (middle) were measured by RT-qPCR or Western blot, respectively, using anti-FLAG and anti-UNR antibodies. The arrowhead denotes a degradation product of UNR-FLAG. The asterisks indicate non-specific bands. A quantification of the number of colonies is shown at the right (n=6).

(D) Analysis of anoikis resistance upon UNR depletion. Cells were grown in flat bottom ultra low attachment plates and growth was documented by bright field microscopy. Spheroid number and area were quantified using ImageJ (n=4).

(E) Cell viability measurements, determined by luciferase-based ATP assays (left) and Caspase3/7 activity normalized to cell viability (right).

(F) Impact of UNR depletion on the invasive capacity of melanoma cells. Spheres were grown in round bottom ultra low attachment plates and further embedded in matrigel. Spheroid area and invasion into the matrigel were quantified by ImageJ. The invasion index was assessed by calculating the ratio area of +dox/-dox (n=4).

(G) Analysis of UACC-257 cell migration and invasion after UNR over-expression. Left, cells were embedded into a 4 mg/ml collagen I matrix and their migration analyzed by time-lapse microscopy; n, nº cells analyzed in at least three different experiments. See also Movie S2. Right, cell spheres were obtained and treated as in F.

(H) Analysis of anoikis resistance (top) and invasion (bottom) upon UNR depletion or over-expression in a number of cell lines of different tumor origins. UNR was depleted by either inducible shRNA expression (shU) or transfection of siRNA pools (siU) for 72 h. A control shRNA (shC) or siRNA pool (siC) were used in parallel. Over-expression was achieved by lentiviral transduction of constructs expressing UNR (+U) or GFP (+G) (n=3). Cell names, tumor origins (M, melanoma; BC, breast cancer; OC ovarian cancer), and BRAF mutations are indicated at the bottom.

Error bars depict the standard deviation of independent experiments. Significance was estimated by Student's T-test (p value * ≤ 0.05, ** ≤0.01, *** ≤ 0.001).

Movie S1, Related to Figure 1. Migration of SK-Mel-103 cells upon UNR depletion
Movie S2, Related to Figure 1. Migration of UACC-257 cells upon UNR over-expression

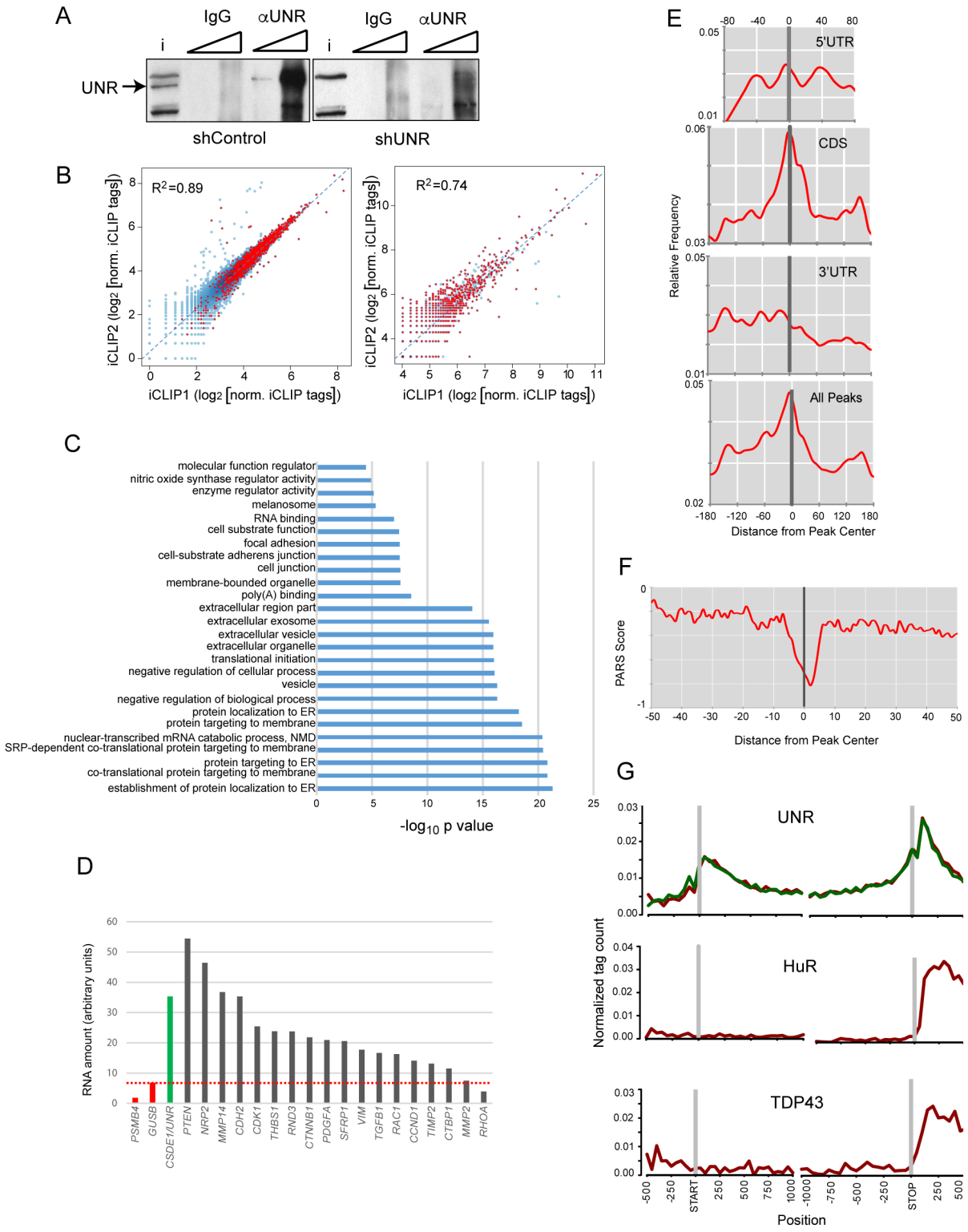

Figure S3. Identification of UNR Targets by iCLIP-Seq (Related to Figure 3)

(A) Characterization of the anti-UNR antibody. Control and UNR depleted cell extracts were used to immunoprecipitate UNR, carrying IgG as negative control. i, input. Increasing amounts of eluate were loaded.

(B) Scatterplots showing the correlation between two independent iCLIP experiments. Left, Correlation of iCLIP tags within genes. Red dots denote genes with called Peaks in both experiments. Right, Correlation of iCLIP tags in called peaks. Red dots denote localized Peaks (i.e. peaks with tag density >4x above average tag density across the mRNA). Tag numbers are normalized for experiment coverage. R2 denotes the correlation coefficient.

(C) Gene Ontology (GO) analysis of UNR iCLIP targets. The most significant terms are indicated.

(D) Validation of the iCLIP results by RT-qPCR in independent RNA immunoprecipitation (RIP) experiments. The amount of RNA normalized to input is shown. Red, negative controls; green, positive control; dashed line, threshold for enrichment.

(E) Relative frequency of the UNR binding signature ([C/G/U]AAG[A/U]A) around iCLIP peaks.

(F) Secondary structure determination around UNR binding peaks. Experimental PARS scores were obtained from Wang et al (Nature 2014).

(G) Metagene analysis of UNR iCLIP density reads along the mRNA. Two other RBPs binding mature mRNA, HuR and TDP43, are shown as comparison.

Table S1, Related to Figures 3-5. Provided as an Excel file
Table S2, Related to Figure 3. Provided as an Excel file
Table S3, Related to Figure 3. Provided as an Excel file
Table S6, Related to Figures 3-5. Provided as an Excel file.

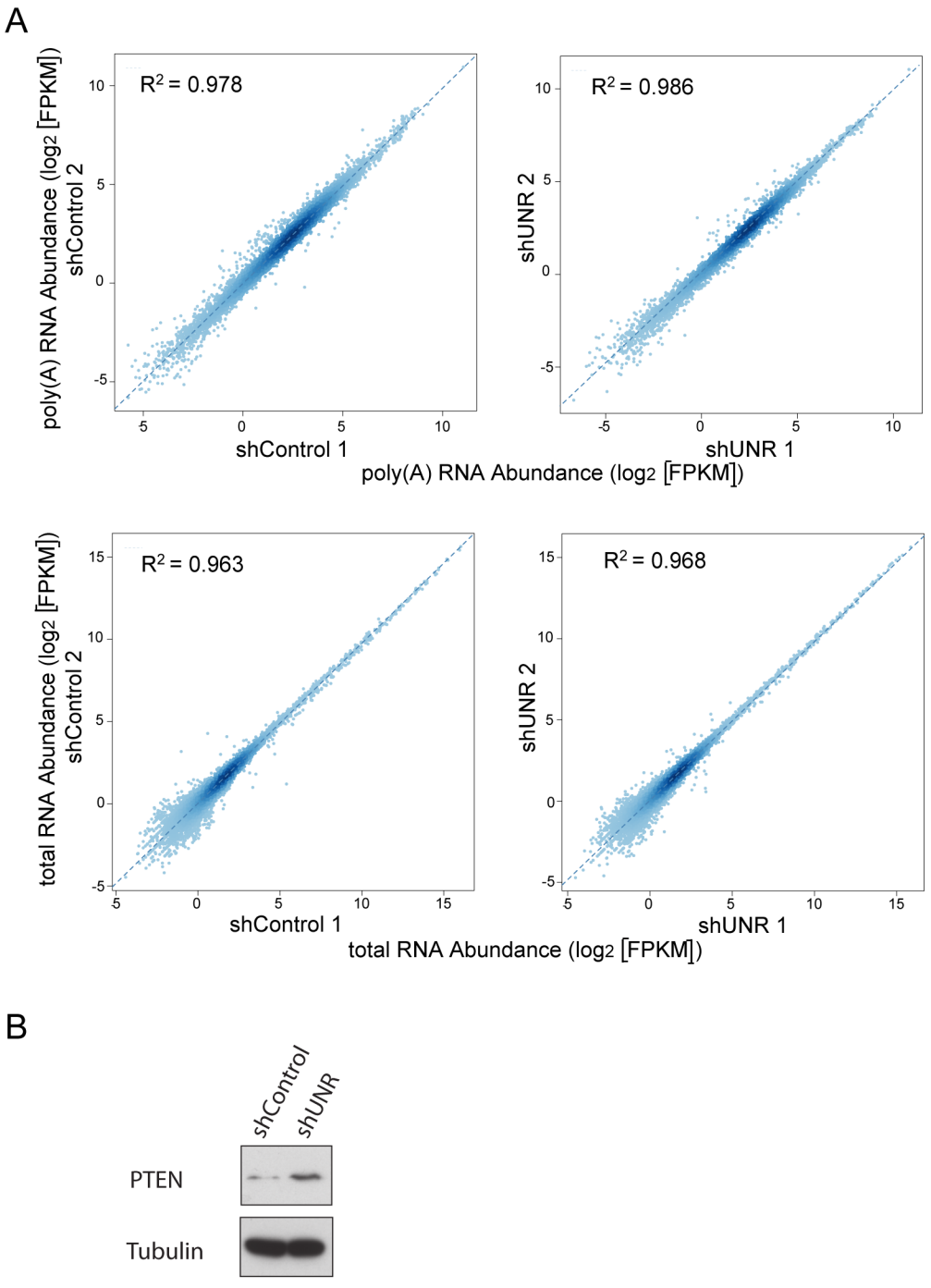

Figure S4. Regulation of mRNA Levels by UNR (Related to Figure 4)
(A) Scatterplots showing the correlation of gene abundance estimates across RNA-seq replicates.
(B) Analysis of PTEN protein levels upon depletion of UNR.

Table S4, Related to Figure 4. Provided as an Excel file

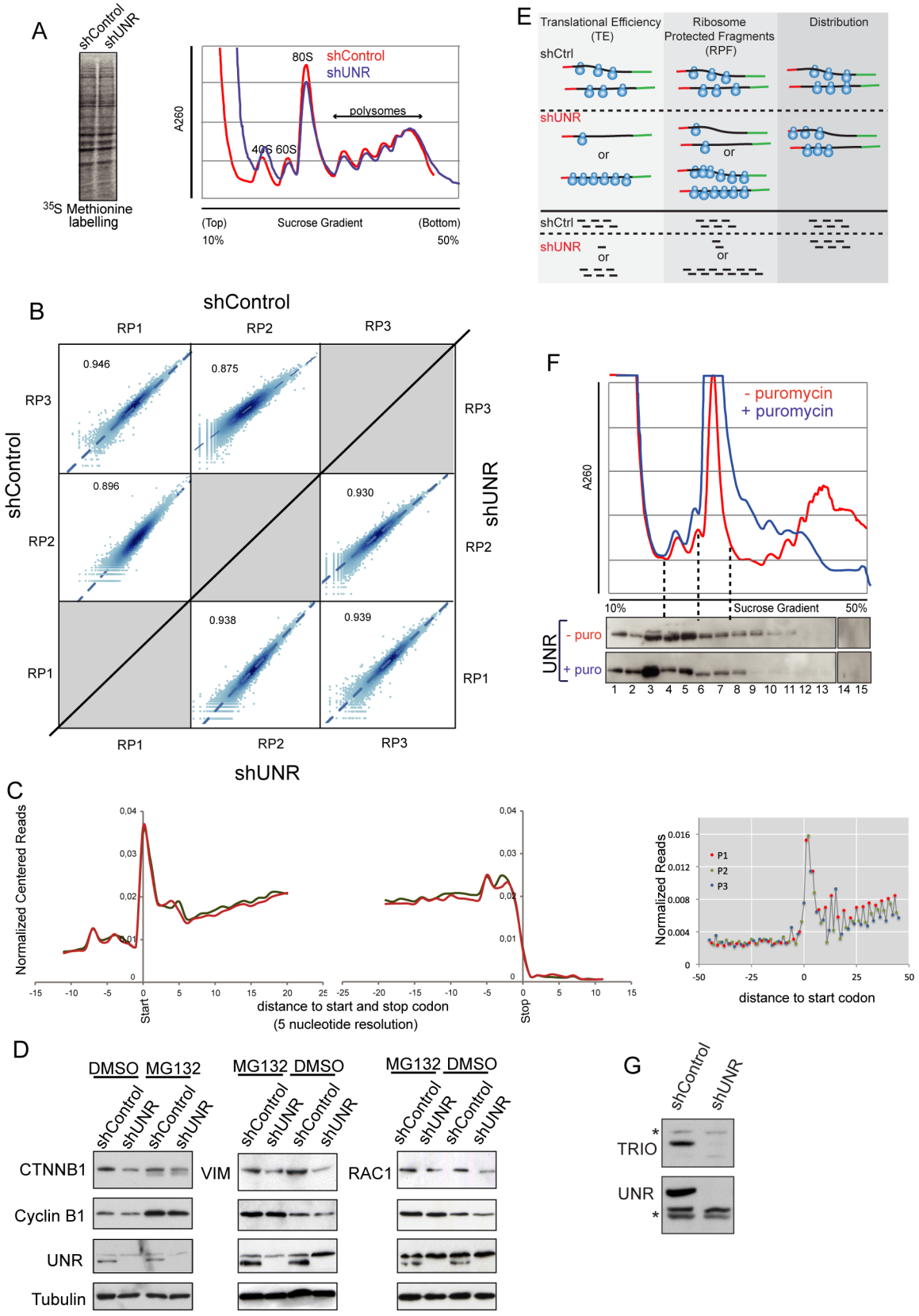

Figure S5. Polysome Analysis and Ribosome Profiling (Related to Figure 5).

(A) Left, de novo protein synthesis in control and UNR depleted cells, assessed by metabolic labeling with 35S-Methionine. Right, polysome profiles of control and UNR depleted cells. The 40S, 60S, 80S and polysome peaks are indicated.

(B) Scatterplots showing the correlation of gene read density across three ribosome profiling replicates (RP1, RP2 and RP3). Values denote the correlation coefficient.

(C) Left, metagene analysis of ribosomes binding along the transcript at 5 nucleotide resolution. Green, shControl; Red, shUNR. Right, metagene analysis of RPF1 (shCtrl) at one nucleotide resolution exhibiting frame periodicity. P1, P2, P3 indicate reading frames 1, 2 and 3, respectively.

(D) Impact of UNR depletion on the levels of CTNNB1, VIM and RAC1. The levels of these factors were assessed in the presence or absence (DMSO) of the proteasome inhibitor MG132. Cyclin B1 was used as a positive control for upregulation upon proteasome inhibition, while tubulin was used as loading control.

(E) Schematic representation of the ribosome profiling analysis (see supplementary methods for details). Black lines, CDS; green lines, UTRs. Ribosome protected fragments (RPFs) are represented in the lower part of the cartoon.

(F) Analysis of UNR association to polysomes. Sucrose gradients were performed in the presence or absence of puromycin, and the presence of UNR along the gradient was analyzed by Western blot.

(G) Analysis of TRIO levels upon UNR depletion. Asterisks denote unspecific signals that serve as loading controls.

Table S5, Related to Figure 5. Provided as an Excel file
Table S7, Related to Figure 6. Provided as an Excel file

SUPPLEMENTAL EXPERIMENTAL PROCEDURES

WET-LAB PROCEDURES:

Constructs

Lentiviral constructs expressing shControl or shUNR were obtained from Dharmacon (TRIPZ shControl (RHS4743); TRIPZ shCSDE1 clone ID V2THS_212077 (RHS4696-200681476)). For over-expression experiments, human UNR open reading frame (a gift from Anne Willis, UK) was cloned with a C-terminal Flag-tag in the CSI emerald lentiviral expression vector using UNR Flag-Fw and UNR Flag-Rev oligonucleotides, or in the MSCV-Pig retroviral vector using UNR-MSCV-Fw and UNR-MSCV-Rev oligonucleotides (see oligonucleotide list). For rescue experiments, three silent point-mutations were introduced at the shUNR complementary site of the UNR-CSI emerald construct with the Quick Change Site Directed Mutagenesis kit (Agilent Technologies) using UNRrescueFw and UNRrescueRev primers. LOXL2 CDS fused to a C-terminal FLAG tag was cloned into an MSCV retroviral vector (a gift from Sandra Peiró, IMIM, Barcelona). Vimentin and Rac1 CDS fused to a C-terminal FLAG tag were cloned into the CSI Emerald lentiviral vector using VIM-Rescue-Fw and VIM-Rescue-Rev primers, and Rac-Rescue-Fw and Rac-rescue-Rev primers, respectively.
For transfection experiments, the full-length VIM-3'UTR was amplified from SK-Mel-103 total RNA using oligos VIM-3UTR-LUC-F and VIM-3UTR-LUC-R, and cloned into the BamHI site of the Firefly Luciferase cassette (Coll et al., 2010) using the Gibson isothermal assembly method (Gibson et al., 2009). All constructs were verified by sequencing.

Cell culture and UNR depletion

Human melanoma, ovarian and breast cancer cell lines were cultured at 37°C in Dulbecco's Modified Eagle Media (DMEM) supplemented with pyruvate (Invitrogen), 10% foetal bovine serum (FBS) and 1% penicillin-streptomycin. Transformed but non-tumoral Mel-ST cells (a kind gift of Corine Bertolotto) were grown in similar conditions using 7% FBS. Primary human melanocytes were isolated from neonatal foreskins (obtained from the Hospital Niño Jesús, Madrid, Spain), and cultured as described (Denoyelle et al., 2006). Melanocytes were maintained in Medium 254 supplemented with melanocyte growth factors (HMG-1) containing 10ng/ml phorbol 12-myristate 13-acetate (Invitrogen).
To deplete UNR, melanoma cells were infected with lentiviral particles expressing shControl or shUNR (see "constructs" section for reference number) essentially as previously described (Alonso-Curbelo et al., 2014). After selection with 1 µg/ml puromycin, co-expression of shRNA and red fluorescent protein (RFP) was induced by adding 0.5 µg/ml doxycycline to the medium. All experiments were performed after at least 3 days of shRNA induction. For high-throughput assays, shRNA expression was induced for 5 days.
Depletion with siRNA pools (siTools, Martinsried, Germany) was obtained by transfection of $5x10^5$ cells using 9 µl Lipofectamine RNAiMax and 5 nM of the indicated siRNA pools according to the manufacturer's instructions. siTools siRNA pools consist of 30 individual non-overlapping siRNAs directed against UNR (siUNR) or non-human sequences (siControl), each with a final concentration of 0.6 nM to avoid RNAi off-target effects (Hannus et al., 2014). Cells were split 24 hr post-transfection to allow expression and phenotypic analyses from the same transfection.
For the cumulative growth assays shown in Figure 2A, $1x10^5$ cells were plated in triplicate. Every two days, the cells were counted and $1x10^5$ cells were redistributed again in new wells. The number of counted cells were added up for each data point in the curve (0= day 0 cells; 2= day 0 + day 2 cells; 3= day 0 + day 2 + day 4 cells, etc).

Cell transfections

shControl or shUNR cells were transfected with mRNA synthesized using MEGAscript® T3 Transcription Kit (Ambion, Cat No. AM1338). Transfections were carried out with 1.5 pmol of mRNA per well of a 6-well plate using the TransMessenger Transfection Reagent (Qiagen, Cat No. 301525). Luciferase activity was measured 4 hr after transfection using Dual-Luciferase® Reporter Assay System (Promega, Cat No. E1910). Firefly luciferase activity was normalized by the amount of transfected mRNA detected by RT-qPCR using LucFlr-F and LucFlr-R primers and by total protein amount.

Cell extracts, Western blot, immunoprecipitation and antibody generation

Cell extracts were prepared by homogenization in HNTG buffer (20mM Hepes pH 7.9, 150 mM NaCl, 1% Triton, 10% glycerol, 1mM MgCl2, 1mM EGTA, 1X protease inhibitors from Roche) or total lysis buffer (50 mM TRIS-HCl pH 7.4, 50 mM NaCl, 1% SDS, 2 mM $MgCl_2$). The homogenate was spun 10 min at 13Krpm and the supernatant was snap-frozen and stored at -80°C.
For UNR immunoprecipitation (IP), 300 µg of protein from total melanoma cell extracts were incubated with 20 µl of protein A magnetic dynabeads (Invitrogen) bound to 2.5 µg of anti-UNR antibody or rabbit IgG in 500 µl of IPP buffer (20 mM Hepes pH 7.9, 150 mM NaCl, 1.5 mM $MgCl_2$, 0.5 mM DTT, 0.05 % NP-40) for 1 hr under rotation at 4°C. Beads were washed 5 times with 5 volumes of IPP and incubated for 10 min at 96°C in 20 µl SDS loading buffer. Proteins were resolved by SDS-PAGE and visualized by Western blot.
Recombinant full-length UNR was expressed as a His-tagged fusion and used to generate antibodies in rabbits. The antibody was affinity purified against UNR columns, and characterized by Western blot and immunoprecipitation of melanoma cell extracts.
The following antibodies were used in Western blot and/or IP: our affinity purified anti-UNR antibody, anti-UNR rabbit polyclonal (Abcam ab96124), anti-Tubulin mouse monoclonal (Sigma, T9026), anti-Vimentin mouse monoclonal (Novocastra, NCL-L-VIM-V9 or BD Transduction Laboratories), anti-CTNNB1 mouse polyclonal (BD Transduction Laboratories), anti-PTEN (goat polyclonal Santa Cruz N19, or rabbit polyclonal Cell Signalling), anti-Rac1 mouse polyclonal (BD Transduction Laboratories), anti-TRIO rabbit polyclonal (Santa Cruz, H120), and anti-Flag mouse monoclonal (Sigma, M2).

Immunohistochemistry (IHC)
Human melanoma samples were obtained from the CNIO Biobank. These included normal skin (n=2), benign lesions (intradermal, congenital and dysplastic/Spiz nevi; n= 10, 5 and 6, respectively), primary cutaneous, mucosal and choroidal melanoma (n= 17, 2 and 1, respectively), as well as lesions metastatic to the skin or the lymph nodes (n= 20). Formalin-fixed, paraffin embedded biopsies were cut and incubated with Pt link (Dako) for 20 min at 95 °C in a high pH buffered solution (EnVision Dako kit). To block endogenous peroxidase, holders were incubated with peroxide for 10 min (EnVision Flex peroxidase blocking reagent). Biopsies were stained with commercial rabbit polyclonal anti-UNR antibody (Abcam, ab96124) at a 1:50 dilution during 20 min and with secondary antibody ("labelled polymer" EnVision FLEX/HRP, Dako) for 20 min. IHC were revealed with 3,3´-diaminobenzidine (DAB, Dako) for 10 min. To provide contrast, a counterstaining was performed with hematoxylin (EnVision Flex, Dako) for 5 min. IHC scoring was performed blind, and linkage to clinical data was performed only after all analyses were completed. The specimens were classified as low, medium or high-intensity UNR staining.

Growth and clonogenic assays
To assess growth, melanoma cells were distributed in triplicates into 24-well plates (10.000 cells per well in 500 µl of growth medium supplemented with doxycycline), trypsinized along 7 days and counted in a Neubauer chamber. To measure cumulative growth, 100.000 cells were distributed in triplicates in 6-well plates with 2 ml of growth medium supplemented with doxycycline. Every two days, cells were trypsinized, counted in a Neubauer chamber, diluted and redistributed in new plates to count again after 2 days, over a period of 10 days.
For clonogenic assays, 500 cells were distributed in 6-well plates as described above. When colonies were visible, cells were washed with PBS and stained with 0.5% crystal violet (made in 25% methanol) for 1 hr.

Soft agar colony formation assay
Eight hundred µl of agar (1.17% noble agar, Difco) in DMEM + pyruvate + 10% FBS + 5% penicillin/streptomycin were distributed in wells of 10-well plates. After solidification, 10.000 cells were mixed with 0.315 % agar in the same solution containing 0.5 µg/ml doxycycline, and added on top of the agar. After 10 min of incubation at room temperature, 1 ml of complete growth medium with 0.5 µg/ml doxycycline was added, and plates were incubated at 37°C. Growth medium was renewed every 3 days and colonies were stained with 0.005% iodonitrotetrazolium chloride (Sigma-Aldrich) and counted. Number and colony area (total/well) were quantified using ImageJ.

Anoikis assay
Cells transiently transfected with siRNA pools, or stably transduced with shRNA or over-expressing constructs were used. Cells were incubated with 0.5 µg/ml doxycycline for 3-4 days before assessing anoikis. One thousand cells (in quadruplicates) were seeded in flat bottom ultra low attachment plates (Corning) and incubated in the presence of 10% FBS (Figure 2D and S2D) or 1% FBS for more stringent

conditions. Doxycycline (0.5 µg/ml) was additionally added to transduced cells. After 4 days, anoikis resistant cells formed spheroids which were documented by bright field microscopy (4x magnification). Number and spheroid area (total/well) were quantified using ImageJ. Cell viability was determined by luciferase-based ATP measurements (Cell titre glo kit, Promega). Caspase3/7 activity was measured via the Caspase glo kit (Promega) and normalized to cell viability.

Invasion assay
Spheroid formation was carried out in round bottom ultra-low attachment plates (Corning) 3-4 days after doxycycline addition using the Spheroid invasion kit (Cultrex) with 2000 cells/spheroid. After 3 days in the presence of doxycycline, basal membrane extract invasion matrix (BME) was added. After gelation, DMEM + pyruvate + 10% FBS + 5% penicillin/streptomycin + 0.5 µg/ml doxycycline were added. Spheroid invasion was monitored over 4 days by bright field microscopy. The final spheroid area after 4 days was quantified using ImageJ and normalized to the initial area (at the time of BME addition) to correct for initial size differences. The invasion index was assessed by calculating the area ratio of doxycycline+/doxcycycline- for either shControl or shUNR cells. Four spheroids from 2 independent experiments were analyzed.

Migration assays
To assess single cell migration in a 3D environment, cells were embedded into a 4 mg/ml collagen I gel (Millipore). Cell spreading was allowed for 12-16 hr before time lapse microscopy using a TCS-SP5X confocal laser scanning microscope (Leica) was used to follow cell movement (interval: 10 min; total: 10 hr). Cells were detected based on their intrinsic fluorescence or using the CellMask deepred life dye (Thermo Fisher) using white light laser excitation by the respective wavelengths, hybrid detectors, 20x magnification and standardized settings. 3D cell tracking was performed using IMARIS Track and surface segmentation. The mean speed of migration was determined by the total tracked path over time. Only cells tracked for at least 2 hr were considered.

Mouse xenografts
Melanoma cells expressing shUNR or shControl were divided into 2 groups for incubation in vehicle or doxycycline for 3 days. One million cells in 400 µl PBS were injected subcutaneously, bilaterally into the flanks of 8 week-old athymic nude/Foxn1 mice. Ten mice were used per condition. Doxycycline was added to the drinking water (1g/l doxycycline; 75g/l sucrose) in order to maintain the depletion levels of UNR. Drinking water was changed every 3 days. After approximately 20 days, tumors were resected and weighted. For the in vivo metastasis assays, xenografts were generated in 6-week old female nu/nu mice *(Crl:NU(Ico)Foxn1nu)* by subcutaneous implantation of $1x10^6$ cells of the indicated cell lines. To allow for the analysis of metastatic dissemination, the cells were transduced with a luciferase reporter. Tumor growth was monitored every two days by measuring the two orthogonal external diameters of the tumor using a caliper. Tumor volume was calculated using the formula (a x b2 x 0.52). Tumors were grown until they reached a size of 1.5 cm^3, when animals were sacrificed. Fifteen minutes before animals were sacrificed, 150 mg/kg of luciferin (Perkin Elmer, Baesweiler Germany) were injected intraperitoneally. After sacrificing, the sentinel (inguinal) and distal (axillary and brachial) lymph nodes at both sides of the animal were extracted and analyzed for the presence of metastatic cells using an IVIS-SPECTRUM imaging system. Luciferase activity was presented in photons per second per square centimeter per steradian (radiance).

Lung extravasation assay
Melanoma shControl or shUNR cells were infected with retroviral particles containing a luciferase reporter for constitutive expression of luciferase (pMSCV-Luc2-PGK-Neo-IRES-GFP). Cells were selected for gentamicin resistance (0.5 mg/ml G418, Sigma) and shRNA expression was induced for 3 days. These cells were injected into the tail vein of 12 week-old female nu/nu mice (*Crl:NU(Ico)Foxn1nu*), at an amount of $1.5x10^6$ cells/mice in 0.1 ml PBS (n= 5 mice per condition). Doxycycline was maintained in the drinking water at concentration of 0.8 mg/ml ad libitum. Five animals were injected per condition. Two mice were euthanized at day 3 after injection to visualize early events of extravasation, and the remaining animals were sacrificed at day 43 and 59 to assess the ability to form efficient lung metastases. Mice were monitored once weekly for luciferase imaging as a readout of metastatic colonization (see below). Four additional mice were injected in the shUNR group and sacrificed at days 72 and 96 to visualize late metastasis. Even at these time points, UNR depletion did not give rise to detectable tumors (data not shown). Lungs were processed for histology upon perfusion with 10% formalin through the trachea. Serial sections were performed for each lung (50 sections, 3 mm

thickness) and ALU II hybridization (Roche, ref. 780-2221) was performed every other 10 sections. Lung architecture was analyzed by standard hematoxylin and eosin (H&E) staining.
Non-invasive imaging of luciferase was performed using an IVIS-SPECTRUM imaging system (Perkin Elmer). Animals were anesthetized with isoflurane and injected intraperitoneally with 150 mg/kg luciferin (Perkin Elmer). Sequential images were obtained after luciferin injection and the maximum light emission was determined for each animal as previously described (Martinez-Corral et al., 2012). Photons emitted from specific regions were quantified using Living Image software (Caliper Life Sciences). In vivo luciferase activity is presented in photons per second per square centimeter per steradian (radiance).

iCLIP-Seq
iCLIP was performed as described (Konig et al., 2011). Briefly, shControl melanoma cells cultured in 10 cm plates were washed with 4 ml cold PBS, 2ml of PBS were added and cells were irradiated at 240 nm on ice with an energy of 150 mJ/cm^2 using a UVC 500 UV Crosslinker (Hoefer). Cells were collected and centrifuged for 3 min at 3000 rpm. The pellet obtained from 2.5 plates was resuspended in 500 µl of iCLIP lysis buffer (50 mM Tris-HCl pH 7.4, 100 mM NaCl, 1% Igepal CA-630, 0.1% SDS, 0.5% sodium deoxycholate). The cell lysate was sonicated using a bioruptor (Digenode) for 3 cycles of 30 s at level H. RNA was then partially digested by adding 1 U of RNase I (Ambion, AM2295), as well as 4 U of Turbo DNase (Ambion, AM 2238). After 3 min of incubation at 37°C under shaking at 1100 rpm, the lysate was incubated on ice for 5 min, centrifuged 10 min at 15000 rpm and the supernatant was collected. For pre-clearing before immunoprecipitation, 500 µl lysate were diluted with 1500 µl iCLIP lysis buffer supplemented with 2 µl SUPERase-In (Ambion, AM2694) and incubated in presence of 50 µl of naked protein A magnetic Dynabeads (Invitrogen) for 30 min under rotation at 4°C. For immunoprecipitation of UNR-RNA complexes, 5 µg of anti-UNR affinity purified antibody were covalently crosslinked to 40 µl of protein A Dynabeads. The pre-cleared lysate was incubated with the anti-UNR beads or with beads with IgG as control, during 1 hr under rotation at 4°C. cDNA libraries were produced as in (Konig et al., 2011) and sequenced by Solexa using a a HiSeq 2000, Single Read, 50 nt at the EMBL Genomics Core facility in Heidelberg. Data were analyzed as described in computational methods.

RNA-Seq from PolyA and total RNA
RNA was recovered from shControl and shUNR melanoma cells induced with doxycycline for 5 days, by Trizol (Ambion) extraction and RNA precipitation. For PolyA RNA-Seq, libraries were prepared using the TruSeq Stranded mRNA Sample Prep Kit v2 (Illumina ref. RS-122-2101/2) according to the manufacturer's protocol. For total RNA-Seq, 5 µg of total RNA were depleted of ribosomal RNA using the Ribo-Zero rRNA removal kit (Epicentre, MRZH116). The resulting RNA was then used for library preparation using the TruSeq small RNA Sample Prep Kit (ref. RS-200-0012, Illumina) according to the manufacturer's protocol. After purification on gel and amplification, final libraries were analyzed using Agilent DNA 1000 chip to estimate the quantity and check size distribution, and were then quantified by qPCR using the KAPA Library Quantification Kit (ref. KK4835, KapaBiosystems) prior to amplification with Illumina's cBot. Libraries were sequenced using a HiSeq 2000, Single Read, 50 nt at the CRG Genomics Facility. Data were analyzed as described in computational methods.

Ribosome profiling
Ribosome profiling was performed according to the protocol described in (Ingolia et al., 2012). Briefly, shControl and shUNR melanoma cells were cultured in 10 cm plates and induced with doxycycline for 5 days. New medium supplemented with 100 µg/ml cycloheximide (Sigma-Aldrich; C4859) was added to 3 plates. After 3 min incubation, cells were washed with ice cold PBS and 250 µl of lysis buffer (20 mM Tris-HCl pH 7.4, 150 mM NaCl, 5 mM $MgCl_2$, 1 mM DTT, 100 µg/ml cycloheximide, 1% Triton-X100) were added. Cells were then collected in one tube and incubated on ice. Glass beads (Sigma-Aldrich; G8772) were added to the lysate and cells were broken by vortexing at medium speed for 3 pulses of 10 s. After 10 min of incubation on ice, lysates were centrifuged for 5 min at 5000 rpm at 4°C, and the supernatant was recovered. RNA was partially digested with 3.5 µl of RNase I (100 U/µl, Invitrogen AM2294) per 800 µl of lysate. After 15 min of incubation at 24°C, lysates were placed on ice and supplemented with 10 µl of SUPERase In (20 U/µl, Invitrogen AM2694). Lysates were then loaded on a 34% sucrose cushion (34% sucrose in 20 mM Tris-HCl pH 7.4, 150 mM NaCl, 5 mM $MgCl_2$, 1 mM DTT and 100 µg/ml cycloheximide) and monosomes were pelleted by centrifugation for 4 hr at 70000 rpm using a Beckman TLA 100.3 rotor. RNA was extracted from the pellet and ribosome protected fragments (RPF) of 30 nucleotides were purified as described (Ingolia et al., 2012). RPFs were depleted of ribosomal RNA with the Ribo-Zero rRNA removal kit (Epicentre MRZH116) according to manufacturer's indications. cDNA libraries were generated according to (Ingolia et al., 2012) and

sequenced by Solexa using a HiSeq 2000, Single Read, 50 nt at the EMBL Genomics Core facility in Heidelberg. Data were analyzed as described in computational methods.

RNA-Immunoprecipitation (RIP)

Cells cultured in 10 cm plates were washed with PBS and resuspended in 200 µl lysis buffer (100 mM KCl, 5 mM $MgCl_2$, 10 mM HEPES pH 7.9, 0.5% NP40, 1 mM DTT, 100 U/ml RNasin, 1X protease inhibitor cocktail (Roche)). The suspension was incubated for 5 min on ice, sonicated in a bioruptor (Digenode) for 3 cycles of 30 seconds at level H, and centrifuged for 10 min at 13000 rpm at 4°C. Eight hundred µg of the supernatant were pre-cleared by adding 50 µl of naked Dynabeads in 1000 µl of NT2 buffer (50 mM Tris-HCl pH 7.5, 150 mM NaCl, 1 mM $MgCl_2$, 0.05% NP40, 200 U/ml RNasin, 1 mM DTT, 20 mM EDTA) and incubating for 30 min under rotation at 4°C. The pre-cleared extract was incubated for 1 hr under rotation at 4°C, with 40 µl of protein A magnetic beads containing anti-UNR antibody or rabbit IgG as control. These beads were prepared as follows: 40 µl beads were blocked with 50 ng/µl tRNA for 15 min at room temperature, and subsequently bound to 5 µg of anti-UNR antibody or to rabbit IgG for 30 min at room temperature. Excess antibody was washed with IPP 500 (20 mM Hepes pH 7.9, 500 mM NaCl, 1.5 mM $MgCl_2$, 0.5 mM DTT, 0.05% NP40) and beads where equilibrated with NT2 buffer. After incubation with the extract, beads were washed 4 times with 1 ml of NT2 buffer and bound RNA was recovered by phenol chloroform extraction and RNA precipitation in presence of 0.5 µl of glycoblue (Ambion). RNA was also extracted from the input lysate and precipitated.

Reverse Transcription and quantitative PCR

RNA from RIP experiments, or 5 µg of total RNA for RNA-Seq validation, was DNase-treated in a final volume of 50 µl using the TURBO DNase kit (Ambion) following the vendor's instructions. Five µl of DNase-treated RNA (corresponding to 500 ng of total RNA) were reverse transcribed in a volume of 20 µl using the Superscript II kit (Invitrogen) in the presence of 2.5 µM oligo(dT), 2.5 ng/µl degenerated N6 oligonucleotides and 50 U of Superscript II, at 42°C for 50 min. The resulting cDNA was diluted ¼ and analysed by quantitative PCR using SYBR Green I Master Mix (Roche) with the Roche LightCycler480 System.

For analysis of RIP experiments, the amount of precipitated RNA was normalized to the amount of the RNA in the input (arbitrary units). For validation of RNA-Seq experiments, gene expression was normalized to either *GUSB* or *PSMB4*, which were used as negative controls. The log_2 ratio of the normalized RNA amount in shUNR versus shControl cells was calculated and plotted. For quantification of the RNA present in UNR rescue cells, an arbitrary amount of RNA in shControl cells was considered as 100%, and the relative amount of RNA in UNR depleted and rescue cells was calculated.

Polysome gradients

Cells (3x 10 cm plates) were incubated with fresh medium supplemented with 100 µg/ml of either cycloheximide or puromycin (Sigma). Cycloheximide cells were incubated for 2 min at 37°C, while puromycin cells were incubated for 5 min. Cells were then washed with ice cold PBS supplemented with 100 µg/ml cycloheximide and resuspended in 250 µl lysis buffer (10 mM Tris-HCl pH7.4, 100 mM KCl, 10 mM $MgCl_2$, 1% Triton-X100, 2 U/ml Turbo DNase (Ambion), 2 mM DTT, 10 U/ml RNasin (Promega), 100 µg/ml of cycloheximide). Glass beads (Sigma-Aldrich; G8772) were added to the lysate and cells were broken by vortexing at medium speed for 3 pulses of 10 s. After 5 min of incubation on ice, the cell lysate was centrifuged for 5 min at 5000 rpm at 4°C. The supernatant was collected and the absorbance was measured at 260 nm with the NanoDrop. Ten-fourteen A_{260} units were loaded onto a 10-50% sucrose gradient (see below). Polysomes were separated by centrifugation at 35000 rpm for 3 hr using a Beckmann SW41 rotor. Fifteen fractions of 800 µl were collected while polysomes were monitored by following the absorbance at 254 nm. Total protein was retrieved by ethanol precipitation and analysed by SDS-PAGE followed by Western blot.

Sucrose gradients were obtained by adding 6 ml of 10% sucrose over a layer of 6ml 50% sucrose prepared in lysis buffer without Triton and containing 0.5 mM DTT, in a 12 ml tube (Polyallomer; Beckman Coulter). Gradients were obtained with the help of a gradient maker (Gradient Master, Biocomp).

Metabolic labelling

Cells were distributed in triplicate wells of a 6-well plate ($6x10^5$ cells/well). After 24 hr, new growth medium supplemented with 10 µCi ^{35}S-Methionine was added, and the cells were incubated for 1 hr at 37°C. Cells were then washed with PBS and lysed in HNTG buffer (20 mM HEPES pH 7.9, 150 mM NaCl, 1% Triton, 10% glycerol, 1 mM $MgCl_2$, 1 mM EGTA, 1x Protease inhibitors (Roche)). The lysate was centrifuged at 13000 rpm and the supernatant recovered. Fifteen µg of total protein extract was

analysed by SDS-PAGE. The signal was visualized in a Typhon reader (Typhoon TRIO variable Mode Imager, Amersham Biosciences).

Polysome run-off

Polysome run-off assays were performed by labeling nascent polypeptides using click-chemistry. shControl and shUNR cells were cultured for 2 hr in the absence of L-Methionine and L-Cysteine (DMEM Gibco 21013). Click-it L-homopropargylglycine (HPG, Invitrogen C10186) was added to the medium at a concentration of 40 µM and labeling of newly synthetized proteins allowed to proceed for 2 hr. Translation initiation was then inhibited with 2 µg/ml Harringtonine for 10 min. Samples were collected at this time (t= 0) and after further 10 min had spanned (t= 10 min). Cells were washed several times with PBS and scraped. After centrifugation at 5000 rpm, the cell pellets were lysed in 300 µl of TRIS-HCl pH 8.0 + 1% SDS. Lysates were sonicated and protein concentration was measured by Bradford. Equal amounts of total protein were labeled with Biotin azide (Invitrogen B10184) following the instructions of the Click-it Protein Reaction Buffer kit (Invitrogen C10276). Labeled proteins were selected with streptavidin beads, and resolved by SDS-PAGE. Newly synthesized proteins were detected by Western blot.

Proteasome inhibition

Cells cultured in 10 cm plates were replenished with new medium supplemented with 50 µM of MG132 (Sigma-Aldrich, C2211) or with DMSO as negative control. After 7 hr, cells were washed with PBS and lysed in HNTG buffer. The lysate was centrifuged at 13000 rpm and the supernatant recovered and analysed by Western blot.

List of oligonucleotides

Oligonucleotide	**5'-3' Sequence**
UNR Flag-Fw	CA GGATCC ATG GGC TTT GAT CCA AAC CTT CTC CAC AAC
UNR Flag-Rev	CA GGATCC TCA CTT GTC ATC GTC ATC CTT GTA ATC GTC AAT GAC ACC AGC
UNRrescueFw	GAC TTA AAA GTA GGA GAT GA**C** GT**C** GA**G** TTT GAA GTA TCA TCG GAC
UNRrescueRev	GTC CGA TGA TAC TTC AAA **C**TC **G**AC **G**TC ATC TCC TAC TTT TAA GT
UNR-MSCV-Fw	CGCCGGAATT AGATCT ATG GGC TTT GAT CCA A ACCTTCTCCACAAC
UNR-MSCV-Rev	TGACGATGACAAG TGA AGATCTCTCGAGGTTA
Rac-rescue-Fw	CA GGATCC ATG CAG GCC ATC AAG TGT GTG GTG GTG GGA
Rac-rescue-Rev	CA GGATCC TCA CTT GTC ATC GTC ATC CTT GTA ATC CAA CAG CAG GCA TTT
LucFlr-F	TTGTTTCCAAAAAGGGGTTG
LucFlr-R	CATCGACTGAAATCCCTGGT
VIM-3UTR-LUC-F	CAAATTGTAAAGATCTAAATTGCACACACTCAGT
VIM-3UTR-LUC-R	ATCCGTTAACAGATCTCCAAAGATTTATTGAAGCA G
Vim Fw	GGAGGAAATGGCTCGTCACC
Vim Rev	CTGCTCTCCTCGCCTTCCAG
VIM-rescue-Fw	CAGGATCCATGTCCACCAGGTCCGTGTCCTCGTCC
VIM-Rescue-Rev	CAGGATCCTCACTTGTCATCGTCATCCTTGTAATCT TCAAGGTCATCGTG
CTBP1 Fw	GTCCTGAACGAGGCTGTGGG

CTBP1 Rev	ACTGCCAATCCGGACGATG
MMP14 Fw	TGCCTGCGTCCATCAACACT
MMP14 Rev	CTTGGGGTAGCCAGGTTCCA
MMP2 Fw	GTGAAGTATGGGAACGCCGA
MMP2 Rev	TGGTGGAGCACCAGAGGAAG
Timp2 Fw	GCCAAAGCGGTCAGTGAGAA
Timp2 Rev	GGAGGGGGCCGTGTAGATAA
Rac1 Fw	GGAGAAGAAGCTGACTCCCATCA
Rac1 Rev	CTGTCTTGAGGCCTCGCTGT
RhoA Fw	ATGATGAGCACACAAGGCGG
RhoA Rev	TACCCAAAAGCGCCAATCCT
CDK1 Fw	TTTCAGAGCTTTGGGCACTCC
CDK1 Rev	GGGATGCTAGGCTTCCTGGTT
CDH2 Fw	GCGTGTGAAGGTTTGCCAGT
CDH2 Rev	GGATGATGATGCAGAGCAGGA
PDGFA Fw	AGCAGTGTCAAGTGCCAGCC
PDGFA Rev	CCGGATTCAGGCTTGTGGTC
PSMB4 Fw	CCTCTGGCGACTACGCTGATTT
PSMB4 Rev	CCATCTCCCAGAAGCTCCTCATC
GusB Fw	CAAGCATGAGGATGCGGACA
GusB Rev	GCTGGTACGGAAAGCGTTGG
SFRP1 Fw	ACGGTGTGTCCTCCCTGTGA
SFRP1 Rev	AGTGCAAACTCGCTGGCACA
TGFB1 Fw	GCAACAATTCCTGGCGATACCT
TGFB1 Rev	AACCACTGCCGCACAACTCC
CCL2 Fw	ATCACCAGCAGCAAGTGTCC
CCL2 Rev	TGGAATCCTGAACCCACTTC
LOXL2 Fw	CAACGTGGCCAAGATTCAG
LOXL2 Rev	AGCGTGGATGGAGAAGTCGT
TNC Fw	CAATCCAGCGACCATCAAC
TNC Rev	AACGGTGTCTTCCAGAGCAG
Smek1 Fw	TGGCATGGATGATACACAGG
Smek1 Rev	GCCTCCTGCATGACAAACTC
NPAS2 Fw	TATCAACCCAGGGTCCAAAG
NPAS2 Rev	GGGACACTAGGCTGCTTCCA
LATS2 Fw	ATGCTGCAGGAACTGGTGAA
LATS2 Rev	CAGGTAGCCCATCTTGCTGA
Adam32 Fw	CAGATCCACTGGCTGTCAAA
Adam32 Rev	CATGTGCTGAAGCCTTAATTATCC
S100A10 Fw	AAAGACCCTCTGGCTGTGGA
S100A10 Rev	GGCCCGCAATTAGGGAAA
Timp3 Fw	CCTGCTACTACCTGCCTTGCTT
Timp3 Rev	CCAGGGTAACCGAAATTGGAG
ITGB8 Fw	ACTGGGCCAAGGTGAAGACA
ITGB8 Rev	CTCTTGAACACACCATCCACATTC

PTPRF Fw	CCCATGGTGACAGCAAACCT
PTPRF Rev	CCTGTAGCTTGGCACACGAA
UNR Fw	ACACAGACTGAGTACCAAGGA
UNR Rev	CCTTTCTGCAGGCAATCCC
RND3 Fw	GTCCTATGACCAGGGGGCAA
RND3 Rev	CCAAGGTGGCAACGTGAAAA
THBS1 Fw	GAAGATGGCCACCAGAACAA
THBS1 Rev	CATCATCGTGGTCACAGGCA
Nrp2 Fw	TCCTCATCACCATCATCGCC
Nrp2 Rev	AGCTCAGGCCCGAGTAGGAA
PTEN Fw	ACAAAGCCAACCGATACTTTTCTC
PTEN Rev	GAAGTTGAACTGCTAGCCTCTGG
CCND1 Fw	CAATGACCCCGCACGATTT
CCND1 Rev	ACAGAGGGCAACGAAGGTCTG

COMPUTATIONAL METHODS

iCLIP-Seq

Raw sequence reads were demultiplexed and adapter remnants were trimmed using cutadapt (Martin 2011). Reads were mapped on the hg19/GRCh37 version of the human genome using bowtie2 (Langmead and Salzberg, 2012) and command line arguments:

--trim5 9 --very-sensitive

The 9 additional 5' nucleotides trimmed during mapping correspond to the reads' assigned barcode (3 random nucleotides + 4 experimental barcode nucleotides + 2 random nucleotides). Post-mapping only reads with a unique best-scoring alignment were kept. Reads mapping on the same coordinates were corrected for amplification bias based on their random barcodes. Specifically for each coordinate the corrected read count C is estimated as:

$C = U \cdot \max(\tilde{N}, 1)$

where U and $\tilde{N}$ denote the number of unique barcodes and the median count of reads per each of the possible 256 barcodes. Due to the high frequency of sequencing errors at the 5' end of the reads a barcode is considered unique if it has no neighbors with hamming distance $d<3$ and a higher read count.

For example for the random barcodes, read count pairs:

ACGGT{9}, TCGAT{1}, AGGGT{2}, GCCTT{6}, GCCCT{1}, AGTAA{1}

only three barcodes are considered as unique (ACGGT, GCCTT, AGTAA) and the median count of reads across all possible 256 barcodes is 0 and so:

$C = 3 \cdot \max(0,1) = 3$.

Nucleotide resolution and 5nt-smoothed bedGraph files for the crosslink sites were generated for each replicate. Peaks of iCLIP tags were called using the HOMER software suite (http://homer.salk.edu/) with command line arguments:

-i backgroundTagDir -tbp -0 -center -region -size 6 -minDist 12 -P 1e-8 -strand separate -fragLength 5

where backgroundTagDir is the HOMER tag directory generated from the merge of the Mock shRNA polyA+ sequencing replicates. Finally "localized" peaks were identified as those having >4x enrichment over the average iCLIP tag density across the corresponding mRNA.

For motif analysis iCLIP-peak (see peak calling section) overlapping tags were first extended 10 nt in each direction of the crosslink site. Non-mRNA-overlapping sequences were removed and sequence k-tuples from identical loci were collapsed to ensure a more even representation of the UNR-bound sequence space. The remaining sequences were used as input to the DREME tool of the MEME package (v4.9.1) for short ungapped motif discovery (Bailey et al. 2011) using a di-nucleotide shuffled instance of the input as background and with command-line parameters:

-norc –g 200 –mink 4 –maxk 7

Motif analysis was performed both with and without hard-masking of sequences containing stretches of repetitive elements yielding near-identical results.

RNA-Seq from PolyA and total RNA

Raw sequence reads were demultiplexed and adapter remnants were trimmed using cutadapt (Martin 2011). Processed reads were aligned with Tophat2 (Kim et al., 2013) on the hg19/GRCh37 human genome and the corresponding UCSC transcriptome with command line parameters:
--no-novel-juncs -g 1 --b2-very-sensitive
shControl and shUNR samples were analyzed for differential gene expression using Cuffdiff2 (Trapnell et al., 2013) with default parameters. A change is considered significant if the p value < 0.005 (for polyA RNA) < 0.01 (for total RNA).

Ribosome profiling
To obtain the maximum information of our ribosome profiling (RP) data, three sets of analysis were performed. First, we quantified crude, normalized ribosome protected fragments (RPFs) along each CDS in shUNR versus shControl cells excluding transcripts that changed at the steady state level. This analysis provides a list of transcripts likely regulated at translation initiation with consequences on final protein output. Second, we considered all transcripts and normalized the number of RPFs with their RNA levels, yielding a category of mRNAs that change at their translational efficiency (TE). TE analysis reveals changes in translational control, but is blind to compensatory effects. For instance, mRNAs present in reduced amounts that are translated more efficiently would score positive in this category, although this situation may not result in different amounts of translated product. Third, we analyzed the distribution of ribosomes along the mRNA, revealing transcripts that, even with the same RPFs in control versus UNR depleted cells, showed accelerated or slower elongation/ termination.
Raw sequence reads were demultiplexed and adapter remnants were trimmed using cutadapt (Martin 2011). Processed reads were size-selected in order to enrich for ribosome-protected fragments and those between 22 and 36 nt, corresponding to ~90% of the total reads recovered from all the replicates, were kept for subsequent analysis.
Reads derived from rRNAs and tRNAs were filtered out after a first pass mapping using bowtie2 and a custom composite rRNA/tRNA genome. Remaining reads were aligned with Tophat2 on the hg19/GRCh37 human genome and the corresponding UCSC transcriptome. “Crude” RPF values for individual RPF replicates were calculated considering only reads overlapping the canonical CDS according to UCSC annotation. Differential “crude” RPF counts were calculated using the DEseq bioconductor R package (Anders and Huber, 2010).
TE values for individual RP replicates were calculated by normalizing RPF-derived CDS DEseq counts to the merged replicate polyA+ or total RNA (for histone genes) CDS DEseq counts of the corresponding condition (shControl or shUNR). Specific A-site positions were assigned using the offset from the 5’ end of the read that maximized codon position periodicity quantified as the difference of median densities between codon sites +1 and +2.
Significant differences in distribution of ribosome footprints across the transcripts between the shControl and shUNR conditions of individual RP replicates were calculated by applying the two-sample Smirnov-Kolmogorov test on binned fragment counts for the two conditions along the CDS as well as 5’ and 3’ UTR flanks of no more than 75 nt. Bins were of variable size *s* depending on the length of the total analyzed sequence *l (s=12+l/40*).
In each category (Crude RPF, TE and Distribution) we considered a gene positive when it showed the same trend in 2 out of 3 RP experiments. Of these, we considered only genes with $\log_2$ fold change > 0.5 (i.e. 1.5 fold change) and p value < 0.2 in both experiments.

Assignment of coordinates to genomic features
For all genome wide RNA-Seq, iCLIP-Seq and Ribosome profiling analyses, coordinates were assigned to genomic features (5’ and 3’ UTRs, CDS, Introns) according to the canonical UCSC annotation (Karolchik et al., 2014) for the hg19/GRCh37 human genome.

PARS-scores analysis
Calculation of normalized PARS scores for human renatured transcripts was performed using data and procedures from (Wan et al 2014).

Gene Ontology Analyses
For all gene ontology analyses, the GOrilla tool (Eden et al., 2009) was used in the two unranked lists mode and the top 5000 expressed genes in SK-MEL-103 cells according to the total RNA-Seq in the shControl condition used as background.

Network construction

A curated list of 74 melanoma genes (Table S7) was created by retrieving relevant genes from the MelGene (Athanasiadis et al., 2014), Cosmic Cancer Gene Census (Futreal et al., 2004), KEGG CANCER (Kanehisa and Goto, 2000; Kanehisa et al., 2014) databases and by adding additional genes selected from the literature: *MIF* (Oliveira et al., 2014), *YBX1* (Schmid et al., 2013), *CYR61* (Dobroff et al., 2009), *CCL2* (Wojnarowicz et al., 2012), *FN1* (Novak et al., 2015), *B2M* (del Campo et al., 2014), *TRIO* (Vaque et al., 2013), *SDC4* (Chalkiadaki et al., 2009), *TNC* (Grahovac et al., 2013), *CTTN* (Tsunoda et al., 2011), *FN1* (Olbryt et al., 2011), *PTEN* (Conde-Perez and Larue, 2012), *RAC1* (Krauthammer et al., 2012), *VIM* (Qendro et al., 2014), *CXCL8* (Singh et al., 2010), *MAPRE1* (Schober et al., 2009; Strickland et al., 2015; Tsao et al., 2012). This list was intersected with UNR regulated iCLIP targets, and interactions between factors of the two lists were identified with the help of Pathway Commons (Cerami et al., 2011). An interaction network was built using the Cytoscape 3.1.1 platform (Shannon et al., 2003).

SUPPLEMENTAL REFERENCES

Alonso-Curbelo, D., Riveiro-Falkenbach, E., Perez-Guijarro, E., Cifdaloz, M., Karras, P., Osterloh, L., Megias, D., Canon, E., Calvo, T.G., Olmeda, D*., et al.* (2014). RAB7 controls melanoma progression by exploiting a lineage-specific wiring of the endolysosomal pathway. Cancer Cell *26*, 61-76.

Anders, S., and Huber, W. (2010). Differential expression analysis for sequence count data. Genome Biol *11*, R106.

Coll, O., Villalba, A., Bussotti, G., Notredame, C., and Gebauer, F. (2010). A novel, noncanonical mechanism of cytoplasmic polyadenylation operates in Drosophila embryogenesis. Genes Dev *24*, 129-134.

Conde-Perez, A., and Larue, L. (2012). PTEN and melanomagenesis. Future Oncol *8*, 1109-1120.
Chalkiadaki, G., Nikitovic, D., Berdiaki, A., Sifaki, M., Krasagakis, K., Katonis, P., Karamanos, N.K., and Tzanakakis, G.N. (2009). Fibroblast growth factor-2 modulates melanoma adhesion and migration through a syndecan-4-dependent mechanism. Int J Biochem Cell Biol *41*, 1323-1331.

del Campo, A.B., Kyte, J.A., Carretero, J., Zinchencko, S., Mendez, R., Gonzalez-Aseguinolaza, G., Ruiz-Cabello, F., Aamdal, S., Gaudernack, G., Garrido, F*., et al.* (2014). Immune escape of cancer cells with beta2-microglobulin loss over the course of metastatic melanoma. Int J Cancer *134*, 102-113.

Denoyelle, C., Abou-Rjaily, G., Bezrookove, V., Verhaegen, M., Johnson, T.M., Fullen, D.R., Pointer, J.N., Gruber, S.B., Su, L.D., Nikiforov, M.A*., et al.* (2006). Anti-oncogenic role of the endoplasmic reticulum differentially activated by mutations in the MAPK pathway. Nat Cell Biol *8*, 1053-1063.

Dobroff, A.S., Wang, H., Melnikova, V.O., Villares, G.J., Zigler, M., Huang, L., and Bar-Eli, M. (2009). Silencing cAMP-response element-binding protein (CREB) identifies CYR61 as a tumor suppressor gene in melanoma. J Biol Chem *284*, 26194-26206.

Eden, E., Navon, R., Steinfeld, I., Lipson, D., and Yakhini, Z. (2009). GOrilla: a tool for discovery and visualization of enriched GO terms in ranked gene lists. BMC Bioinformatics *10*, 48.

Gibson, D.G., Young, L., Chuang, R.Y., Venter, J.C., Hutchison, C.A., 3rd, and Smith, H.O. (2009). Enzymatic assembly of DNA molecules up to several hundred kilobases. Nature methods *6*, 343-345.

Grahovac, J., Becker, D., and Wells, A. (2013). Melanoma cell invasiveness is promoted at least in part by the epidermal growth factor-like repeats of tenascin-C. J Invest Dermatol *133*, 210-220.

Hannus, M., Beitzinger, M., Engelmann, J.C., Weickert, M.T., Spang, R., Hannus, S. and Meister G. (2014). siPools: highly complex but accurately defined siRNA pools eliminate off-target effects. Nucleic Acids Res *42*, 8049-8061.

Karolchik, D., Barber, G.P., Casper, J., Clawson, H., Cline, M.S., Diekhans, M., Dreszer, T.R., Fujita, P.A., Guruvadoo, L., Haeussler, M.*, et al.* (2014). The UCSC Genome Browser database: 2014 update. Nucleic Acids Res *42*, D764-770.

Kim, D., Pertea, G., Trapnell, C., Pimentel, H., Kelley, R., and Salzberg, S.L. (2013). TopHat2: accurate alignment of transcriptomes in the presence of insertions, deletions and gene fusions. Genome Biol *14*, R36.

Martin, M. (2011). Cutadapt removes adapter sequences from high-throughput sequencing reads. EMBnet. journal, 17(1), pp-10.

Martinez-Corral, I., Olmeda, D., Dieguez-Hurtado, R., Tammela, T., Alitalo, K., and Ortega, S. (2012). In vivo imaging of lymphatic vessels in development, wound healing, inflammation, and tumor metastasis. Proc Natl Acad Sci U S A *109*, 6223-6228.

Olbryt, M., Habryka, A., Tyszkiewicz, T., Rusin, A., Cichon, T., Jarzab, M., and Krawczyk, Z. (2011). Melanoma-associated genes, MXI1, FN1, and NME1, are hypoxia responsive in murine and human melanoma cells. Melanoma Res *21*, 417-425.

Oliveira, C.S., de Bock, C.E., Molloy, T.J., Sadeqzadeh, E., Geng, X.Y., Hersey, P., Zhang, X.D., and Thorne, R.F. (2014). Macrophage migration inhibitory factor engages PI3K/Akt signalling and is a prognostic factor in metastatic melanoma. BMC Cancer *14*, 630.

Qendro, V., Lundgren, D.H., Rezaul, K., Mahony, F., Ferrell, N., Bi, A., Latifi, A., Chowdhury, D., Gygi, S., Haas, W.*, et al.* (2014). Large-scale proteomic characterization of melanoma expressed proteins reveals nestin and vimentin as biomarkers that can potentially distinguish melanoma subtypes. J Proteome Res *13*, 5031-5040.

Schmid, R., Meyer, K., Spang, R., Schittek, B., and Bosserhoff, A.K. (2013). Melanoma inhibitory activity promotes melanoma development through activation of YBX1. Pigment Cell Melanoma Res *26*, 685-696.

Schober, J.M., Cain, J.M., Komarova, Y.A., and Borisy, G.G. (2009). Migration and actin protrusion in melanoma cells are regulated by EB1 protein. Cancer Lett *284*, 30-36.

Shannon, P., Markiel, A., Ozier, O., Baliga, N.S., Wang, J.T., Ramage, D., Amin, N., Schwikowski, B., and Ideker, T. (2003). Cytoscape: a software environment for integrated models of biomolecular interaction networks. Genome Res *13*, 2498-2504.

Singh, S., Singh, A.P., Sharma, B., Owen, L.B., and Singh, R.K. (2010). CXCL8 and its cognate receptors in melanoma progression and metastasis. Future Oncol *6*, 111-116.

Strickland, L.R., Pal, H.C., Elmets, C.A., and Afaq, F. (2015). Targeting drivers of melanoma with synthetic small molecules and phytochemicals. Cancer Lett *359*, 20-35.

Tsao, H., Chin, L., Garraway, L.A., and Fisher, D.E. (2012). Melanoma: from mutations to medicine. Genes Dev *26*, 1131-1155.

Tsunoda, K., Oikawa, H., Tada, H., Tatemichi, Y., Muraoka, S., Miura, S., Shibazaki, M., Maeda, F., Takahashi, K., Akasaka, T.*, et al.* (2011). Nucleus accumbens-associated 1 contributes to cortactin deacetylation and augments the migration of melanoma cells. J Invest Dermatol *131*, 1710-1719.

Wojnarowicz, P., Gambaro, K., de Ladurantaye, M., Quinn, M.C., Provencher, D., Mes-Masson, A.M., and Tonin, P.N. (2012). Overexpressing the CCL2 chemokine in an epithelial ovarian cancer cell line results in latency of in vivo tumourigenicity. Oncogenesis *1*, e27.